Green's function approach to the dynamics-controlled truncation formalism: Derivation of the $\chi^{(3)}$ equations of motion

N. H. Kwong
Cooperative Excitation Project, ERATO, Japan Science and Technology Corporation, Optical Sciences Center, University of Arizona, Tucson, Arizona 85721

R. Binder
Optical Sciences Center, University of Arizona, Tucson, Arizona 85721
(Received 2 September 1999)

The dynamics-controlled truncation (DCT) formalism is a successful microscopic approach that describes coherent correlations in optically excited semiconductors. For practical reasons (including numerical evaluations), its application is limited to lowest-order nonlinearities, such as the $\chi^{(3)}$ regime. Therefore, it is not convenient to use this formalism to examine the role played by incoherent many-body effects, such as carrier-carrier scattering and screening. Traditionally, the most powerful approach to study incoherent effects and correlations in highly excited semiconductors is that of nonequilibrium Green's functions (NGF). A combination of the insights and technical advantages provided by the two (NGF and DCT) approaches will lead to a comprehensive microscopic theory for nonlinear optical phenomena in semiconductors. In this paper, we take a first step in this direction by presenting detailed one-to-one relations between the two formalisms within the $\chi^{(3)}$ approximation. Starting from the standard perturbation theory of nonequilibrium Green's functions, we derive the essential minimal order factorization theorems, to arbitrary order, of DCT and the equations of motions for the interband polarization and the ''biexcitonic'' correlation function. This lays the foundation for future diagrammatic high-intensity generalizations of the DCT formalism.

I. INTRODUCTION

The dynamics-controlled truncation (DCT) formalism[1–5] is a successful microscopic approach that describes coherent phenomena in optically excited semiconductors in the weakly nonlinear (low-density) limit. In each order of the external field, it demonstrates that only a finite set of correlation functions contribute to optical processes and leads to exact, closed equations for the correlation functions. A complete description of all coherent phenomena to certain low orders (e.g., $\chi^{(3)}$) is therefore possible. Its most important application to date has been the elucidation of exciton-exciton correlation effects in femtosecond scale four-wave-mixing experiments in the $\chi^{(3)}$ regime.[5–8]

Despite its successes, DCT's usefulness cannot easily be extended to higher-intensity regimes or situations with pre-excited electrons and holes. All but the lowest-order ($\chi^{(3)}$) evaluation lead to untractable equations of motion, especially with regard to numerical evaluations. Furthermore, questions concerning certain aspects of the formalism remain. For example, it is not clear how incoherent many-body effects enter the description, which precludes a quantitative definition of the time scale of strict validity of the DCT.

Traditionally, the most powerful approach to study all aspects of many-body effects in semiconductors, including both coherent and incoherent effects, have been equilibrium (see, e.g., Refs. 9 and 10) and nonequilibrium (see, e.g., Refs. 11–14) Green's functions. For general treatments of Green's functions see, e.g., Refs. 15 and 16. The applicability of the nonequilibrium Green's functions (NGF) is not limited in intensity or density, but so far it has not been practical to study strong four-body correlations rigorously within this approach.

By combining the advantages of the two (NGF and DCT) approaches, a comprehensive microscopic theory for nonlinear optical phenomena in semiconductors can be developed. In this general theory, the strict validity of the DCT formalism for higher-order nonlinearities will have to be abandoned in order to account for physically relevant high-density effects. Nevertheless, the aim is to keep the benefits of the general theoretical approach of the DCT formalism, namely coupled equations of motion for various expectation values and correlation functions, in such a generalization. Our overall strategy toward this goal is to embed the low-order (at least $\chi^{(3)}$) results of DCT in a diagrammatic perturbative NGF treatment. In this paper we take a first step in this direction, which is to develop a detailed one-to-one correspondence between the two approaches in the $\chi^{(3)}$ limit.

Diagrammatic perturbation theories of Green's functions have been most useful in many-body problems where one can group classes of diagrams, representing certain physical processes, in such a way that their sum can be written as the solution to an integral equation or a differential initial/boundary-value problem. Familiar examples are the Dyson equation for two-point functions and the Bethe-Salpeter equation for the four-point functions with various approximations for the self energies and the irreducible four-point vertices, respectively. The formalism provides a unified framework to examine the various processes quantitatively. Within this framework, the DCT equations to a certain order in the external field should also be representable as the summation of classes of Green's function diagrams. The general idea of relating the DCT formalism to a diagrammatic rep-

 ©2000 The American Physical Society

resentation has already been pointed out and used by Maialle and Sham.[17,18] Some results on the diagrams' properties derived in the present paper were already discussed in Ref. 17. However, for future development, we believe it is important to establish a detailed correspondence between conventional nonequilibrium Green's function diagrams and DCT equations of motion.

In this paper, we examine in detail the standard Feynman-Dyson perturbation theory diagrams for the relevant nonequilibrium Green's functions. In Sec. II, the model Hamiltonian and the Green's functions are defined. The Feynman rules for constructing perturbation theory diagrams for the Green's functions in the electron-hole system are collected in Appendix B. The crucial result from this examination (Sec. III) is that the assumption of an initial ground state annihilates a vast class of diagrams. We classify the nonvanishing diagrams in increasing order of the external field (Sec. IV). In each order up to order three, we show that all nonvanishing terms (to arbitrary order in the two-particle interaction) contributing to the equal-time Green's functions—the density, the polarization, the biexcitonic correlation—can be resummed to yield closed equations of motions that have been derived within DCT. It is intended that these diagrams will be kept in future generalizations to higher densities. Some directions for such generalizations are mentioned in the concluding section.

The formal development of the DCT scheme to arbitrary order in the external field was based on several *factorization* and *contraction* theorems on multipoint density matrices stated and proved in Ref. 3. In Appendix A, going beyond $\chi^{(3)}$, we give diagrammatic proofs of two special cases of these theorems that involve minimal order factorization of two classes of density matrices. Although, as explained above, we are unlikely to extend our present exact identification between the NGF and the DCT formalisms to higher orders in our future development, the purpose of Appendix A is to indicate how one might proceed if one desires to do that.

II. GREEN'S FUNCTIONS ON THE KELDYSH CONTOUR

We work with a model semiconductor system with two groups of bands: conduction and valence bands. In the system's ground state, all the valence bands are filled while the conduction bands are empty. The excited states of the system are described in terms of two species of charged particles: electrons in the conduction bands and holes in the valence bands. We write the Hamiltonian in an arbitrary single-particle basis as follows:

$$\hat{H}=\hat{H}_1+\hat{H}_2+\hat{H}_{ext},$$

$$\hat{H}_1=\sum_{ij}\ \epsilon_e(i,j)a_e^\dagger(i)a_e(j)+\sum_{ij}\ \epsilon_h(i,j)a_h^\dagger(i)a_h(j),$$

$$\hat{H}_2=\frac{1}{2}\sum_{ijmn}\ [\langle ij|V_{eeee}|mn\rangle a_e^\dagger(i)a_e^\dagger(j)a_e(n)a_e(m)$$
$$+\langle ij|V_{hhhh}|mn\rangle a_h^\dagger(i)a_h^\dagger(j)a_h(n)a_h(m)$$
$$+\langle ij|V_{eheh}|mn\rangle a_e^\dagger(i)a_h^\dagger(j)a_h(n)a_e(m)$$

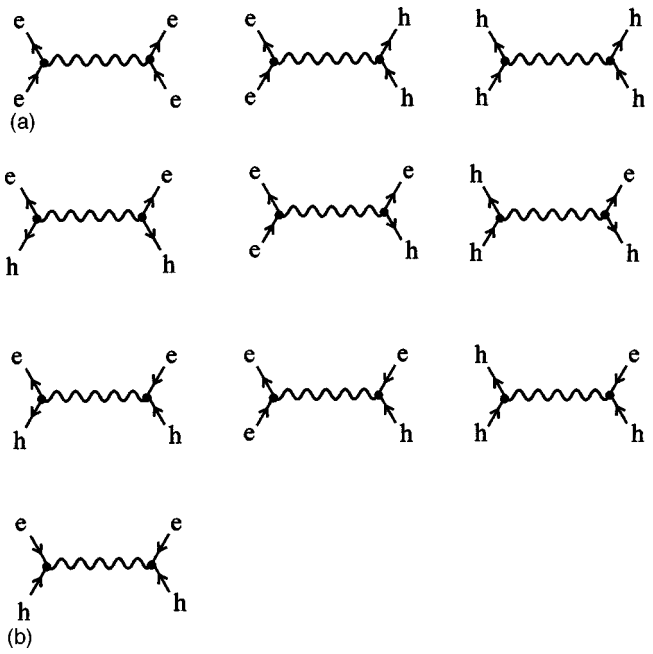

FIG. 1. Matrix elements of a general two-body interaction in a two-component (electrons and holes) plasma. The matrix elements represented by the diagrams in (a) are included in $\hat{H}_2$ in Eq. (1) while those in (b) are not.

$$+\langle ij|V_{hehe}|mn\rangle a_h^\dagger(i)a_e^\dagger(j)a_e(n)a_h(m)]$$

$$\hat{H}_{ext}=\frac{1}{2}\sum_{ij}\ [e^{-i\omega_0 t}\mathbf{E}(t)\cdot\mathbf{d}_{eh}(i,j)a_e^\dagger(i)a_h^\dagger(j)$$
$$+e^{i\omega_0 t}\mathbf{E}^*(t)\cdot\mathbf{d}_{he}(j,i)a_h(j)a_e(i)].$$

Each single-particle orbital is labeled by a species subscript, e or h, and an orbital index that represents the collection of single-particle quantum numbers, e.g., band, momentum, of the orbital. To allow for a general treatment of band coupling, the one-body part $\hat{H}_1$ of the system Hamiltonian is taken to be non-diagonal in the single-particle basis, although it is diagonal in the species label. In $\hat{H}_2$, we have only included those parts of a general electron-electron interaction that do not effect a transition between a conduction band and a valence band, or, equivalently, $\hat{H}_2$ neither creates nor annihilates electron-hole pairs. This approximation is represented graphically in Fig. 1 where all possible types of matrix elements of a two-body interaction are shown. Only the terms represented by Fig. 1(a) are included in $\hat{H}_2$. The justification of this approximation has been discussed in, e.g., Refs. 19 and 20. The ground state of the model system Hamiltonian $\hat{H}_1+\hat{H}_2$ is the electron-hole vacuum provided the binding energy per electron-hole pair in a gas of any density is smaller than the bare band gap, i.e., when the vacuum is stable, which we will assume in the following. The external field Hamiltonian $\hat{H}_{ext}$ only acts to create or annihilate electron-hole pairs. The rotating-wave approximation is taken.

The density matrices that obey the DCT equations of motion, namely the interband polarization p_{eh}, the densities f_{ee} and f_{hh}, and the biexcitonic density matrix B_{eehh}, are defined by:

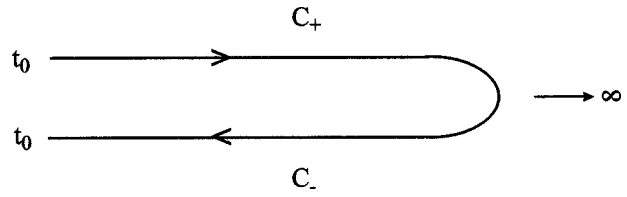

FIG. 2. The Keldysh time contour.

$$p_{eh}(i,j,t)\equiv\langle a_h(j,t)a_e(i,t)\rangle,$$

$$f_{\nu\nu}(i,j,t)\equiv\langle a_\nu^\dagger(j,t)a_\nu(i,t)\rangle$$

$$B_{eehh}(i,j,k,l,t)\equiv\langle a_h(l,t)a_h(k,t)a_e(j,t)a_e(i,t)\rangle,$$

where $\nu=e,h$ and $\langle\cdots\rangle$ denotes averaging with the initial density operator. Here the creation and annihilation operators are Heisenberg picture operators. In this paper we consider a version of the DCT equations in which the mean-field part of the interaction is separated from the correlation part. The four-body dynamical variable in this version is the correlated part of B_{eehh}, defined as

$$\begin{aligned} b_{eehh}(i,j,k,l,t)\equiv B_{eehh}(i,j,k,l,t)&-\langle a_h(l,t)a_e(i,t)\rangle\\ &\times\langle a_h(k,t)a_e(j,t)\rangle+\langle a_h(l,t)a_e(j,t)\rangle\\ &\times\langle a_h(k,t)a_e(i,t)\rangle. \end{aligned}$$

In the $\chi^{(3)}$ regime, the correlation function $b_{eehh}(i,j,k,l,t)$ carries the most interesting physical information, and its properties have been studied extensively from a memory function point of view[21,22] and within DCT.[4–8]

In the NGF formalism, the above density matrices are obtained as equal-time limits of multitime Green's functions ordered along the Keldysh time contour (Fig. 2). The extension to multitime functions facilitates the application of powerful perturbation theory techniques. The two-point Green's functions for our system are defined by

$$\begin{aligned} G_{ee}(i,\overline{t},j,\overline{t'})&=-i\langle T_C[a_e(i,\overline{t})a_e^\dagger(j,\overline{t'})]\rangle,\\ G_{hh}(i,\overline{t},j,\overline{t'})&=-i\langle T_C[a_h(i,\overline{t})a_h^\dagger(j,\overline{t'})]\rangle,\\ G_{eh}(i,\overline{t},j,\overline{t'})&=-i\langle T_C[a_e(i,\overline{t})a_h(j,\overline{t'})]\rangle,\\ \tilde{G}_{eh}(i,\overline{t},j,\overline{t'})&=-i\langle T_C[a_e^\dagger(i,\overline{t})a_h^\dagger(j,\overline{t'})]\rangle, \end{aligned}\tag{2}$$

where the time arguments run along the Keldysh contour (Fig. 2), which starts from the initial time t_0, goes forward along the positive branch C_+ to infinity, and then goes backward along the negative branch C_- to t_0. T_C denotes time ordering along this contour. As above, $\langle\cdots\rangle$ denotes averaging by the initial density operator. In calculations, an alternative representation of the time structure in the Green's functions is often more convenient. Here a time point $\overline{t}$ is represented by (t,b), where t is the ordinary time and $b=+,-$, the Keldysh sign, gives the branch of the contour on which the point resides. Each path-ordered two-point Green's function is then broken down into four components labeled by the Keldysh signs of the two time arguments. For example, the four components of the electron density Green's function G_{ee} are

$$\begin{aligned} G_{ee}^{+-}(i,t,j,t')&=i\langle a_e^\dagger(j,t')a_e(i,t)\rangle,\\ G_{ee}^{-+}(i,t,j,t')&=-i\langle a_e(i,t)a_e^\dagger(j,t')\rangle,\\ G_{ee}^{++}(i,t,j,t')&=-i\langle T_+[a_e(i,t)a_e^\dagger(j,t')]\rangle\\ &=\theta(t-t')G_{ee}^{-+}(i,t,j,t')\\ &\quad+\theta(t'-t)G_{ee}^{+-}(i,t,j,t'),\\ G_{ee}^{--}(i,t,j,t')&=-i\langle T_-[a_e(i,t)a_e^\dagger(j,t')]\rangle\\ &=\theta(t-t')G_{ee}^{+-}(i,t,j,t')\\ &\quad+\theta(t'-t)G_{ee}^{-+}(i,t,j,t'), \end{aligned}\tag{3}$$

where $T_+(T_-)$ denotes time (antitime) ordering along the ordinary time axis. The components of the other Green's functions are written in the same way. For example, the $(++)$ component of the polarization Green's function is

$$G_{eh}^{++}(i,t,j,t')=-i\langle T_+[a_e(i,t)a_h(j,t')]\rangle.\tag{4}$$

Green's functions involving more than two operators are similarly defined. The four-point function corresponding to B_{eehh} is

$$\begin{aligned} G_{eehh}(i,\overline{t},j,\overline{t'},k,\overline{t''},l,\overline{t'''})=(-i)^2\langle T_C[a_e(i,\overline{t})a_e(j,\overline{t'})\\ \times a_h(k,\overline{t''})a_h(l,\overline{t'''})]\rangle. \end{aligned}\tag{5}$$

This function has 16 components in the (t,b) representation. The $(++++)$ component, G_{eehh}^{++++}, for example, has the same expression as Eq. (5) with T_C replaced by T_+. We give the definition of g_{eehh}, the correlated part of G_{eehh}, in Appendix B. It bears the same relation to G_{eehh} as b_{eehh} does to B_{eehh}. Some density matrices and Green's functions with an arbitrary number of external points are also defined in Appendix A.

To analyze and/or calculate the Green's functions, one may follow standard procedures and expand each of them in a time-dependent perturbation series with $\hat{H}_1$ as the unperturbed Hamiltonian. Each term can be represented by a diagram, and the Feynman rules for enumerating these diagrams to arbitrary order and translating them into analytic expressions are stated in Appendix B, to which we also refer the reader for some of the notational and terminological conventions used in this paper. Then, as mentioned above, the density matrices of interest can be obtained as the equal-time limits of particular Green's functions,

$$\begin{aligned} G_{eh}^{++}(i,t,j,t+\epsilon)&=ip_{eh}(i,j,t),\\ G_{ee}^{+-}(i,t,j,t)&=if_{ee}(i,j,t),\\ G_{hh}^{+-}(i,t,j,t)&=if_{hh}(i,j,t), \end{aligned}\tag{6}$$

$$g_{eehh}^{++++}(i,t,j,t+\epsilon,k,t+2\epsilon,l,t+3\epsilon)=-b_{eehh}(i,j,k,l,t),$$

where $\epsilon\searrow 0$. The ambiguity at the equal-time point in the definitions of the Green's function components with all $+$ Keldysh signs calls for the specification of an ordering of the time variables as all of them approach the common time point, as is done here for G_{eh}^{++} and g_{eehh}^{++++}. For these two

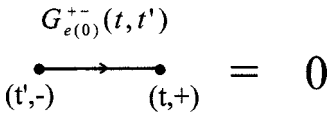

FIG. 3. The $(+-)$ component of the free-particle Green's function, being proportional to the initial density, vanishes.

functions, however, the choice of the ordering is immaterial as these functions are continuous in all time variables at the common time point.

The crucial assumption for the DCT scheme to be valid is that the initial state of the system is the electron-hole vacuum. In our approach, this assumption results in the following expressions for the free-particle (electron or hole) Green's functions:

$$\begin{aligned} G^{+-}_{\nu(0)}(i,t,j,t') &\equiv i\langle a^{\dagger}_{\nu(0)}(j,t')a_{\nu(0)}(i,t)\rangle = 0, \\ G^{-+}_{\nu(0)}(i,t,j,t') &\equiv -i\langle a_{\nu(0)}(i,t)a^{\dagger}_{\nu(0)}(j,t')\rangle \\ &= -i[e^{-(i/\hbar)\epsilon_{\nu}(t-t')}]_{ij}, \\ G^{++}_{\nu(0)}(i,t,j,t') &= \theta(t-t')G^{-+}_{\nu(0)}(i,t,j,t') \\ &= G^{R}_{\nu(0)}(i,t,j,t'), \\ G^{--}_{\nu(0)}(i,t,j,t') &= \theta(t'-t)G^{-+}_{\nu(0)}(i,t,j,t') \\ &= -G^{A}_{\nu(0)}(i,t,j,t'), \end{aligned} \tag{7}$$

where the subscript (0) in the creation and annihilation operators indicates that these are Heisenberg operators evolved by the unperturbed Hamiltonian $\hat{H}_1$, $\nu = e$, h, and ϵ_{ν} is the ν-band single-particle energy matrix in $\hat{H}_1$. The vanishing of $G^{+-}_{\nu(0)}$ (Fig. 3) eliminates many terms in the exact Green's functions' perturbation series. In the following, rules for constructing the surviving graphs are stated and proved. These graphs are then classified by the number of $\hat{H}_{ext}$ vertices. Minimal order factorization theorems, to arbitrary order, of DCT and the DCT equations of motion up to $\chi^{(3)}$ are derived.

III. GRAPHICAL RULES FOR THE CASE OF A VACUUM INITIAL STATE

The rules for drawing perturbation diagrams for our system and translating them into algebraic expressions are collected in Appendix B. As noted above, in the special case of using a vacuum initial state, a large number of diagrams become zero. In this section, we state and prove rules for constructing nonzero graphs. Parts of our terminology, such as particle *segments* and particle *chains*, are not in common usage. For their definitions and those of all graphical elements, the reader is referred to Appendix B. We recall that the full set of labels of the lines and the vertices are time, Keldysh sign, species, and orbital. In order not to unnecessarily clutter the figures or equations, from here on some of the labels not essential to the argument at hand will be omitted. In general we treat an E vertex and an E^* vertex as different vertices. But by saying a certain graph is of order E^n, we mean the total number of external field, E and E^*, vertices is n.

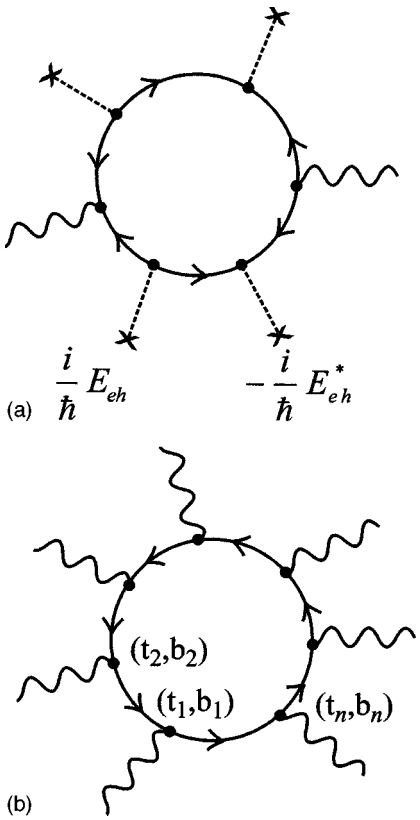

FIG. 4. Examples of closed particle loops.

The validity of the first three rules is actually not limited to situations with initial vacuum states: they are consequences of the fact that $\hat{H}_2$ does not create or annihilate particle-hole pairs at either vertex. Because these rules are repeatedly invoked in later sections, we collect them here for convenience.

Rule 1. Each fermion loop contains an equal number of E vertices and E^* vertices. The E-vertices and the E^*-vertices are placed alternately along the loop [Fig. 4(a)].

Proof. This rule is trivially true for a loop with no $E(E^*)$ vertices. For a loop with external field vertices, start at any particle line and run around the loop in the direction of this line's arrow. By item (B4) in Appendix B, the arrow maintains its direction (V vertices do not switch the arrow's direction) until it meets an external field vertex. By item (B7), the first external field vertex that this line meets must be an E^* vertex. After this vertex, the segment's arrow runs counter to the sense in which we are going around the loop. Since one segment cannot contain two counterpointing arrows, we can see that we must encounter at least one E vertex before returning to the particle line where we started. By the same token, additional E vertices and E^* vertices must appear in pairs, the E^* preceding the E in each pair.

Rule 2. Consider a particle chain connecting two external points in a graph. If both external points correspond to annihilation operators, then the number of E vertices on the chain is one more than that of E^* vertices. If both are creation operators, the excess external field vertex is an E^*-vertex. If the external points are one creation operator and one annihilation operator, then the chain contains an equal number of E-vertices and E^*-vertices.

Proof. The proof is essentially the same as that of Rule 1.

Rule 3. Consider a Green's function that is the expectation value of N annihilation operators and M creation operators ($N+M$ must be an even number). If a contributing graph contains N_E E vertices and N_{E^*} E^* vertices, then the following relation holds:

$$N_E - N_{E^*} = \frac{N-M}{2}.$$

For example, a graph of the density two-point function G_{ee} has an equal number of E vertices and E^* vertices, a graph of G_{eh} has one excess E-vertex, and a graph of G_{eehh} has two excess E vertices.

Proof. By Rule 1, the loops do not contribute to $N_E - N_{E^*}$. Suppose $N>M$. The excess E^* vertices generated by the M creation operators on the chains are matched by the excess E vertices generated by M of the annihilation operators. So the net contribution to $N_E - N_{E^*}$ comes from the extra $N-M$ annihilation operators that are linked by $(N-M)/2$ chains, each of which has one excess E vertex by Rule 2. The same argument applies for $N<M$.

The following rules are valid when the additional assumption of an initial vacuum state is adopted.

Rule 4. If a graph contains a fermion loop that does not contain any external field vertex, the graph $=0$.

Proof. We first consider the special case where the loop is one free-particle line beginning and ending at the same V vertex. In the Wick's factorization of the Green's function, this line comes from the contraction of two operators in the expression for $\hat{H}_2$. Since in this term the creation operators are placed to the left of the annihilation operators, and this ordering is preserved in the T product, the line that results is $\langle a^\dagger_{\nu(0)}(j,t) a_{\nu(0)}(i,t)\rangle = 0$. The more general case is where the loop contains an arbitrary number, say $n(>1)$, of V-vertices, as illustrated in Fig. 4(b). The loop contributes the factor

$$F = \sum_{b_1 b_2, \ldots, b_n = +,-} f(b_1, b_2, \ldots, b_n)$$

$$f(b_1, b_2, \ldots, b_n) = \int_{-\infty}^{\infty} dt_1 \ldots dt_n G^{b_1 b_2}_{\nu(0)}(t_1, t_2) \times G^{b_2 b_3}_{\nu(0)}(t_2, t_3) \cdots G^{b_n b_1}_{\nu(0)}(t_n, t_1) \times V(t_1) V(t_2) \cdots V(t_n)$$

to the graph. For a given sequence of Keldysh signs $(b_1, b_2, \ldots, b_n)$, if any b_i is different from any other b_j, then following the arrow around the loop, we are certain to encounter a $G^{+-}_{\nu(0)}$ and so $f(b_1, \ldots, b_n) = 0$. So the only possible non-zero terms in the sum over the Keldysh signs are $f(+,+,\ldots,+)$ and $f(-,-,\ldots,-)$. For $f(+,+,\ldots,+)$ the integrand contains the factor $\theta(t_1 - t_2)\theta(t_2 - t_3)\cdots\theta(t_n - t_1)$ which reduces the integrand support to a set of measure zero. The same argument applies to $f(-,-,\ldots,-)$. So $F=0$.

Rule 5. This rule concerns a fermion line segment (i.e., it does not contain any $E(E^*)$ vertices), the arrow of which goes from (t', b') to (t, b).

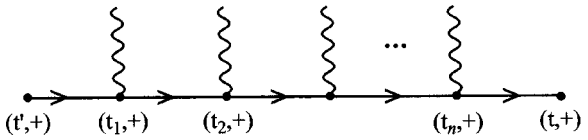

FIG. 5. A particle segment with $(+)$ Keldysh sign on both ends. By Rule 5(b), the Keldysh signs at all intermediate vertices are $+$.

(a) If $b=+$ and $b'=-$, the segment is zero and so annihilates the whole graph.

Proof. In this case, no matter how the intermediate Keldysh signs are assigned, the segment must contain a $G^{+-}_{\nu(0)}$.

(b) If $b=b'=+$, all the intermediate Keldysh signs are $+$, and the time arguments go in increasing order along the direction of the arrow.

Proof. The same argument as in Rule 4 restricts the surviving contributions to those in which all the intermediate Keldysh signs are $+$. Suppose there are n intermediate V vertices. Label them, in the direction from t' to t, $t_1, t_2, \ldots, t_n$ (Fig. 5). Because of the step function in $G^{++}_{\nu(0)}$, these arguments must go in increasing order along the direction of the arrow: $t' < t_1 < t_2 < \cdots < t_n < t$.

(c) If $b=b'=-$, all the intermediate Keldysh signs are $-$, and the time arguments go in decreasing order along the direction of the arrow. The proof is similar to that of Rule 5(b).

(d) If $b=-$ and $b'=+$, a surviving segment is made up of two subsegments: a chain of $-$'s linked to $(t,-)$ and a chain of $+$'s linked to $(t',+)$ connected by a $G^{-+}_{\nu(0)}$ at an intermediate point (Fig. 6). Again the time ordering appropriate to each subsegment applies. The proof is again similar to that of Rule 5(b).

The four parts of the rule can be summarized by the statement that in a surviving segment, the vertices along the arrow's direction must have increasing Keldysh-time arguments.

Rule 6. Any nonzero graph of order E^n contributing to $G^{+-}_{\nu\nu}$, $\nu = e, h$, contains *at most* $n/2-1$ loops. Any nonzero graph of order E^n contributing to $G^{b_1 b_2}_{eh}$ for any b_1, b_2 contains *at most* $(n-1)/2$ loops.

Proof. By Rule 4, a nonzero loop must contain at least one pair of E and E^* vertices. The maximum number of loops is attained if we place exactly one pair in each loop. For $G^{+-}_{\nu\nu}$, n is even by Rule 3. The open chain contains at least one pair of E and E^* vertices. Hence the maximum number of these vertex pairs available to the loops is $n/2 - a$, which is then the maximum number of loops. The argument for $G^{b_1 b_2}_{eh}$ is similar.

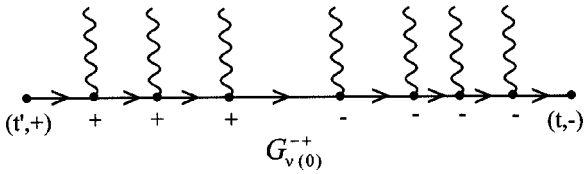

FIG. 6. A particle segment with the arrow going from one end with $(+)$ Keldysh sign to the other end with $(-)$ Keldysh sign. By Rule 5(d), the intermediate vertices are segregated by their Keldysh signs.

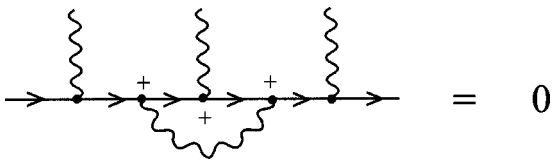

FIG. 7. A graph with a V line connecting two points on the same segment is zero.

Rule 7. If a V line connects two vertices in the same segment, the graph is zero (Fig. 7).

Proof. Consider the subsegment the end points of which are the vertices of the V line in question. The times and Keldysh signs at the two end points must then be the same, and the arrow goes in one direction from one end point to the other. Then the same argument in Rule 4 above that proved the vanishing of a loop with no $E(E^*)$ vertices holds here.

Rule 8. If the end points of a particle segment have equal-time arguments and Keldysh signs, but they are not connected by a V line, then the segment is a noninteracting particle line. In fact, it is equal to zero or the identity matrix in the single-particle basis, depending on from which side of the equal-time point the limit is taken.

Proof. The same argument as in the proof of Rule 4 (the collapsing of the support of the integrand to a zero-measure set) shows that the segment considered here is zero if it contains at least one V vertex. If the whole segment is just one free-particle line, however, since the two points are not connected by a V line, the restriction of operator ordering brought about by $\hat{H}_2$ does not apply. So such a segment may survive. The two possible limiting values for the free-particle line follows from the definitions of $G^{bb}_{\nu(0)}$, Eq. (7).

Rule 9. If two V lines connect the same two segments, the arrows must go in the same direction between the V lines. For example, Fig. 8(a) represents a nonzero graph, while Fig. 8(b) vanishes.

Proof. Consider the two subsegments bounded by the vertices of the two V lines in question in Fig. 8(b). Suppose first the Keldysh signs b_1 and b_2 are different. Then the arrow in one of the two subsegments goes from $-$ to $+$ which annihilates the graph by Rule 5(a). If $b_1=b_2=+$, then by Rule 5(b), the arrows must go in the direction of increasing time in both subsegments, which is impossible. So the graph is zero. The argument is the same for $b_1=b_2=-$.

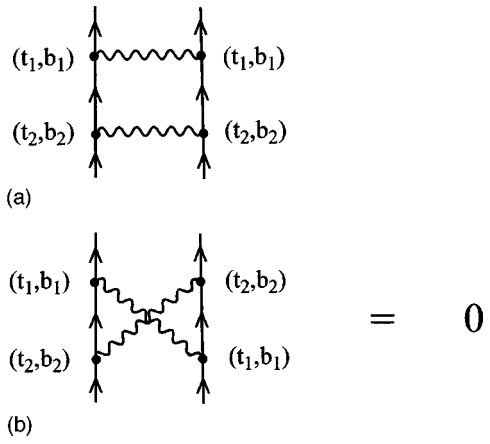

FIG. 8. (a) is nonzero while (b) is zero.

Rule 10. In any nonzero-order (in E) two-point density graph, the $(++)$ component is continuous in each time variable at the point where the two times are equal. In other words, the discontinuity in $G^{++}_{\nu\nu'}(t_1,t_2)$ at $t_1=t_2$ arises entirely from the zeroth-order terms.

Proof. Consider first the case where the open chain is free of $E(E^*)$ vertices. Since, by hypothesis, there are E vertices in the graph, there must be at least one loop. The connectedness of the graph then implies that the open chain must contain some V vertices. Such a chain is then a segment with equal-time arguments and Keldysh signs at both ends, which is zero by Rule 8. So the open chain must contain $E(E^*)$ vertices, in which case it is quite easy to see the graph is continuous at the equal-time point by writing down the analytical expression for the open chain.

IV. THE $\chi^{(3)}$ DYNAMICS-CONTROLLED TRUNCATION EQUATIONS

To derive the $\chi^{(3)}$ DCT equations, we consider the perturbation series of the density matrices p_{eh}, f_{ee}, f_{hh} and the correlation function b_{eehh}, defined in Eq. (6) as the equal-time limit of two-point and four-point Green's functions. For each Green's function, we consider the perturbation graphs that contain up to a fixed number ($\leqslant 3$) of E vertices and any number of V lines. By grouping classes of graphs in certain ways, with the help of the simplifying rules in the previous section, we derive equations of motion for the equal-time Green's functions that are exact to the chosen order in E and which are the same as those derived by DCT.

According to the Feynman rules in Appendix B, certain graphical features, such as the particle label and the arrow direction of a particle segment, are not changed by the addition or subtraction of V lines. It is thus useful, to each order in E, to first consider the graphs with no V lines. We will call them the ''bare'' graphs for that order in E. All graphs can be constructed by ''dressing'' the bare graphs with V lines. This line of analysis was also adopted in Ref. 17.

A. $O(E^1)$ polarization graphs

Although the first-order polarization $G^{++}_{eh}(t,t+\epsilon)$ is trivial, it is economical to clarify its graphical features here since it will appear repeatedly as subgraphs in higher order quantities. By Rule 6, there is only one bare graph which is an open particle chain consisting of one e line and one h line separated by an E vertex [first graph in Fig. 9(a)]. Rule 5 restricts the possible combinations of arrow directions and Keldysh signs to that shown in Fig. 9(a). All contributing graphs are obtained by dressing this bare graph with V lines. By Rule 7, a V line must have one vertex in each of the two segments that are separated by the E vertex. By Rule 9, the V lines cannot ''cross'' each other (Fig. 8). To summarize, the sum of all contributions to $O(E^1)$ is represented by the series shown in Fig. 9(a), which is the bare eh graph dressed by the retarded T matrix of a particle-hole pair in free space.

This (infinite) series of graphs can be efficiently summed by deriving and solving an equation of motion satisfied by the sum. Denoting the sum by $iG^{++(1)}_{eh}(t,t+\epsilon)$, we see from the structure of the graphical series in Fig. 9(a) that it satisfies the following integral equation:

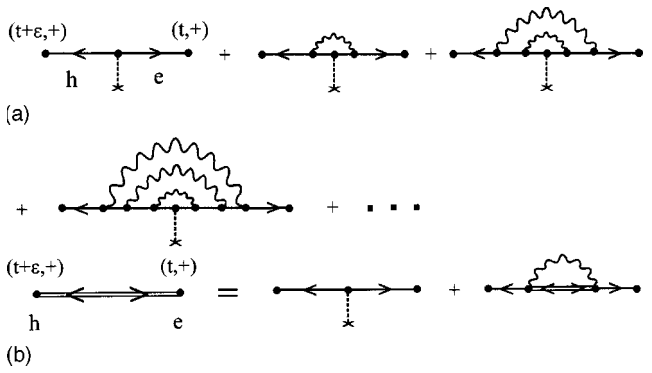

FIG. 9. (a) The diagram series that represent $p^{(1)}_{eh}$. (b) The series in (a) resummed into an integral equation.

$$G^{++(1)}_{eh}(i,t,j,t+\epsilon)=\sum_{m_1 n_1}\int\frac{dt_1}{\hbar}G^{++}_{e(0)}(i,t,m_1,t_1)\times[-E_{eh}(m_1,n_1,t_1)+V^{HF}_{eh}(m_1,n_1,t_1)]\times G^{++}_{h(0)}(j,t+\epsilon,n_1,t_1),\tag{8}$$

where the Hartree-Fock field is given by

$$V^{HF}_{eh}(m_1,n_1,t_1)=i\sum_{m_2 n_2}\langle m_1 n_1|V_{eheh}|m_2 n_2\rangle\times G^{++(1)}_{eh}(m_2,t_1,n_2,t_1).$$

This equation is represented graphically in Fig. 9(b). We now convert Eq. (8) into an equation of motion for the $O(E)$ polarization $p^{(1)}_{eh}(i,j,t)\equiv -iG^{++(1)}_{eh}(i,t,j,t+\epsilon)$. We note that $G^{++(1)}_{eh}$ (and any other two-point Green's functions) is a function of two independent time variables. Therefore, the derivative of its equal-time limit with respect to t is properly defined as

$$\frac{d}{dt}G^{++(1)}_{eh}(i,t,j,t+\epsilon)=\left[\left(\frac{\partial}{\partial\tau_1}+\frac{\partial}{\partial\tau_2}\right)\times G^{++(1)}_{eh}(i,\tau_1,j,\tau_2)\right]_{\tau_1=t,\tau_2=t+\epsilon}.\tag{9}$$

Correspondingly, in differentiating the right-hand side of Eq. (8), we take partial derivatives with respect to t and $t+\epsilon$ in turn, treating them as independent variables, and add the two partial derivatives. Carrying out the differentiation, we obtain, using Eq. (7),

$$i\hbar\frac{d}{dt}p^{(1)}_{eh}(i,j,t)-\sum_{mn}[\epsilon_e(i,m)\delta_{jn}+\epsilon_h(j,n)\delta_{im}]p^{(1)}_{eh}(m,n,t)=E_{eh}(i,j,t)+\sum_{mn}\langle ij|V_{eheh}|mn\rangle p^{(1)}_{eh}(m,n,t),\tag{10}$$

which is of course just the semiconductor Bloch equation in the low-density limit.

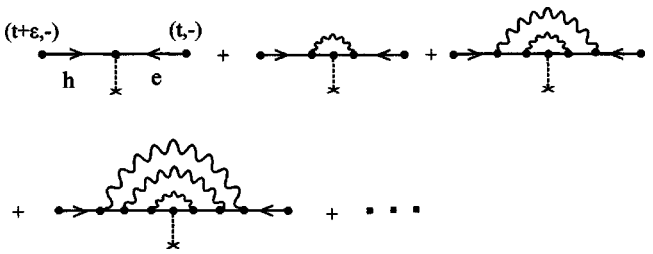

FIG. 10. The diagram series that represents $p^{(1)*}_{eh}$.

It is very useful to regard the above differentiation procedure as applying the inverse operator of the free Green's function, $G^{-1}_{\nu(0)}(i,j,\tau)\equiv i\hbar\partial/\partial\tau\delta_{ij}-\epsilon_\nu(i,j)$:

$$\sum_m G^{-1}_{\nu(0)}(i,m,t)G^{bb'}_{\nu(0)}(m,t,j,t')=\hbar b\,\delta_{bb'}\delta_{ij}\delta(t-t').$$

Equation (10) is the result of applying the operator $G^{-1}_{e(0)}(t)+G^{-1}_{h(0)}(t+\epsilon)$ to Eq. (8). Diagrammatically, on the right-hand side of Fig. 9(b), each of the $G^{-1}_{\nu(0)}$'s acts at an external point where it removes the external $++$ particle line—the line that connects the external point to the rest of the graph—and replace the time and orbital labels on the ''exposed'' vertex by those of the external point.

For later reference, we also note that, from their definitions, $p^*_{eh}(i,j,t)=i\tilde{G}^{--}_{eh}(i,t,j,t+\epsilon)$. A parallel argument as above gives $p^{(1)*}_{eh}$, the $O(E)$ part of p^*_{eh}, as the sum of the graphical series in Fig. 10.

B. $O(E^2)$ density graphs

We consider here the $O(E^2)$ contributions to $G^{+-}_{ee}(t,t)$. The considerations for G^{+-}_{hh} are similar. By Rule 6, there is only one bare graph which is an open particle chain consisting of two e lines and one h line separated by an E vertex and an E^* vertex (Fig. 11). As a result of Rule 5, the only surviving combination of arrow directions and Keldysh signs is the one shown in Fig. 11.

All $O(E^2)$ graphs are obtained by dressing this graph with V lines, the introduction of which is again restricted to certain ways in order to produce a nonzero graph. First, by Rule 5, all graphs have the same three segments as the bare graph, i.e., they have the same particle labels, arrow directions, and Keldysh signs at the $E(E^*)$ vertices. Furthermore, all the V vertices in either e segment are assigned the Keldysh sign of that segment's end points [Rules 5(b) and 5(c)], while the middle h segment is divided into two subsegments with V vertices carrying opposite Keldysh signs [Rule 5(d) and Fig. 6]. By Rule 7, a V line must connect two different segments. Since the two e segments are on different Keldysh branches, no V lines connect them: each V line goes from the h segment to one of the two e segments. These V lines cannot ''cross'' each other. This is true for two V lines going into the same e segment as a result of Rule 8 (Fig. 8). For two V lines going into different e segments, since the

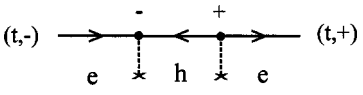

FIG. 11. The bare graph for $f^{(2)}_{ee}$.

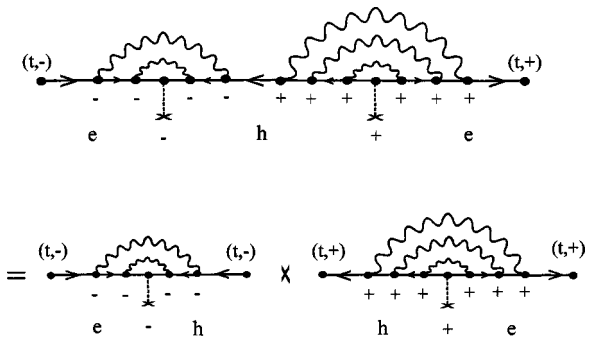

FIG. 12. Factorization of a representative graph of $f_{ee}^{(2)}$ into a product of graphs for $p_{eh}^{(1)}$ and $p_{eh}^{(1)*}$.

two e segments have different Keldysh signs, it is clear that the two V lines cannot cross each other (Fig. 6).

The upshot is that each contributing graph is obtained from the bare graph by dressing the $E(E^*)$ vertices with nonoverlapping sets of V lines (Fig. 12). In such a graph, an h line, given by the factor $iG_{h(0)}^{-+}(t_1,t_2)$, separates the two sets of V lines. Since the vertices at t_1 and t_2 are connected by V lines to the e segments that are bounded by external points at time t, we have $t_1,t_2<t$. From this and the definitions of the free Green's functions in Eq. (7), one may write

$$G_{h(0)}^{-+}(i,t_1,j,t_2)=i\sum_m G_{h(0)}^{--}(i,t_1,m,t+\epsilon) \times G_{h(0)}^{++}(m,t+\epsilon,j,t_2). \tag{11}$$

It is then clear that this density graph can be factorized into two $O(E^1)$ polarization graphs (Fig. 12). Summing over all the contributing graphs, we have

$$f_{ee}^{(2)}(i,j,t)=\sum_m p_{eh}^{(1)*}(j,m,t)p_{eh}^{(1)}(i,m,t), \tag{12}$$

which was derived in DCT and also corresponds to the low-density limit of the Hartree-Fock theory.

C. $O(E^3)$ Polarization Graphs

In this subsection, we will derive the DCT equations for the $O(E^3)$ contributions to the polarization $iG_{eh}^{++}(i,t,j,t+\epsilon)$. By Rule 6, there are two bare graphs: (a) an open chain with two E vertices and one E^* vertex on it [Fig. 13(a)], and

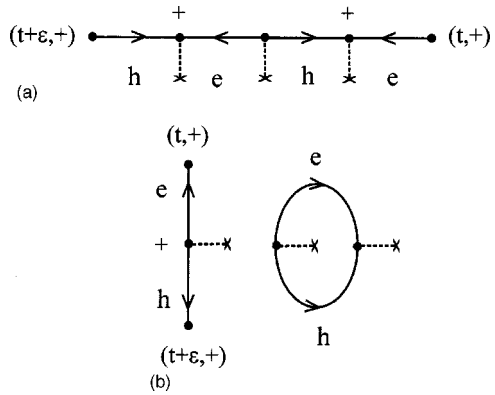

FIG. 13. The bare graphs for $p_{eh}^{(3)}$.

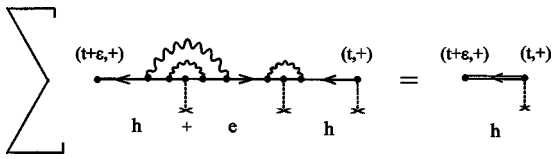

FIG. 14. Summation of Class a(1) graphs. The graph shown on the left is a representative of the series.

(b) an open chain with one E vertex plus one loop containing one E vertex and one E^* vertex [Fig. 13(b)]. Again, all contributing graphs are constructed by dressing these two bare graphs with V lines. Being disconnected, the bare graph (b) itself does not contribute, but its connected dressed versions do. As in Sec. IV A, we will apply inverse (free) Green's functions to derive equations of motion. We will show how the graphs can be grouped so that the sums of individual groups can be identified with terms in the DCT equations.

After the application of $G_{e(0)}^{-1}+G_{h(0)}^{-1}$ (see Sec. IV A), the equation we seek has the following form, with $G_{eh}^{++(3)}(i,t,j,t)\equiv ip_{eh}^{(3)}(i,j,t)$:

$$i\hbar\frac{d}{dt}p_{eh}^{(3)}(i,j,t)-\sum_{mn}[\epsilon_e(i,m)\delta_{jn}+\epsilon_h(j,n)\delta_{im}]p_{eh}^{(3)}(m,n,t) = -i\hbar[\text{all graphs with one external line and one exposed vertex}]. \tag{13}$$

If the exposed vertex is a V vertex, we will refer to the V line emanating from this vertex as the exposed V-line. The two classes stemming from the two bare graphs are considered separately.

Class a. One open particle chain. This class is further divided by physical interpretations into three subclasses:

(1) The exposed vertex is an E vertex. There are two possible ways to assign species indices to the three successive segments: $(h-e-h)$ and $(e-h-e)$. The first way is shown in Fig. 14. According to the Feynman rules, the sum of this set is given by

$$-\frac{1}{\hbar}\sum_m E_{eh}(i,m,t)G_{hh}^{++(2)}(j,t+\epsilon,m,t).$$

By its definition, Eqs. (3) and (6), $f_{hh}^{(2)}(j,m,t)$ is equal to $-iG_{hh}^{++(2)}(j,t,m,t+\epsilon)$ in which the second time argument approaches the first from above—a time ordering opposite to that in $G_{hh}^{++(2)}$ in the above expression. But this difference in time ordering is immaterial since, by Rule 10, $G_{hh}^{++(2)}$ is continuous in time at the equal-time point. Hence the above expression can be written as $i\Sigma_m E_{eh}(i,m,t)f_{hh}^{(2)}(j,m,t)$. Analogous considerations apply to the set with the other species-index assignment. The contributions from the two sets together give the sum of the class as

$$S_{a1}(i,j,t)=-\frac{i}{\hbar}\sum_m [E_{eh}(i,m,t)f_{hh}^{(2)}(j,m,t) + f_{ee}^{(2)}(i,m,t)E_{eh}(m,j,t)], \tag{14}$$

This class represents Pauli blocking to the electron-hole excitation.

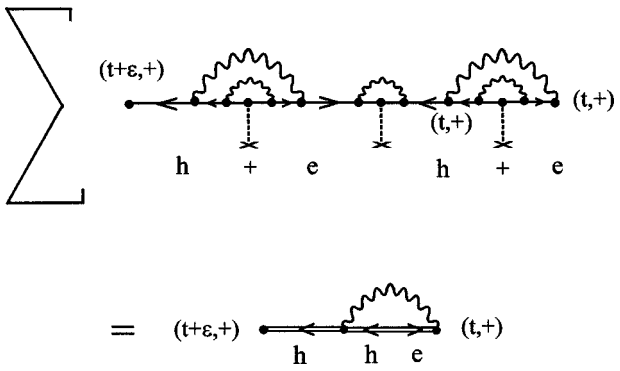

FIG. 15. Summation of Class (a21) graphs, in which the exposed V line ends in the middle h segment. The graph shown on the left is a representative of the series.

(2) The exposed vertex is a V vertex, and the exposed V line is not crossed by any other V lines. These graphs will give the Fock mean-field contributions to the right-hand side of the equation for $p_{eh}^{(3)}$. The sum of this class is given by three terms, each of which corresponds to the sum of a set of graphs in which the exposed V line ends in a particular segment (Figs. 15–17):

$$S_{a2}(i,j,t)=S_{a21}+S_{a22}+S_{a23},$$

$$\begin{aligned} S_{a21}(i,j,t)=&-\frac{i}{\hbar}\sum_{kmn}[\langle ik|V_{eheh}|mn\rangle p_{eh}^{(1)}(m,n,t)f_{hh}^{(2)}(j,k,t) \\ &+\langle kj|V_{eheh}|mn\rangle p_{eh}^{(1)}(m,n,t)f_{ee}^{(2)}(i,k,t)], \end{aligned} \tag{15}$$

$$\begin{aligned} S_{a22}(i,j,t)=&-\frac{i}{\hbar}\sum_{kmn}[\langle in|V_{eeee}|mk\rangle f_{ee}^{(2)}(m,n,t)p_{eh}^{(1)}(k,j,t) \\ &+\langle jn|V_{hhhh}|mk\rangle f_{hh}^{(2)}(m,n,t)p_{eh}^{(1)}(i,k,t)], \end{aligned}$$

$$S_{a23}(i,j,t)=\frac{i}{\hbar}\sum_{mn}\langle ij|V_{eheh}|mn\rangle p_{eh}^{(3a)}(m,n,t),$$

where S_{a21}, S_{a22}, S_{a23} are contributions from Figs. 15, 16, and 17, respectively. $p_{eh}^{(3a)}$ is defined by Fig. 17 and denotes that part of $p_{eh}^{(3)}$ that is given by graphs stemming from the bare graph in Fig. 13(a).

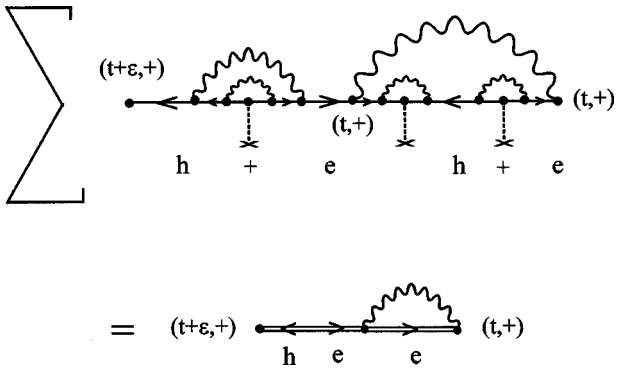

FIG. 16. Summation of Class (a22) graphs, in which the exposed V line ends in the middle e segment. The graph shown on the left is a representative of the series.

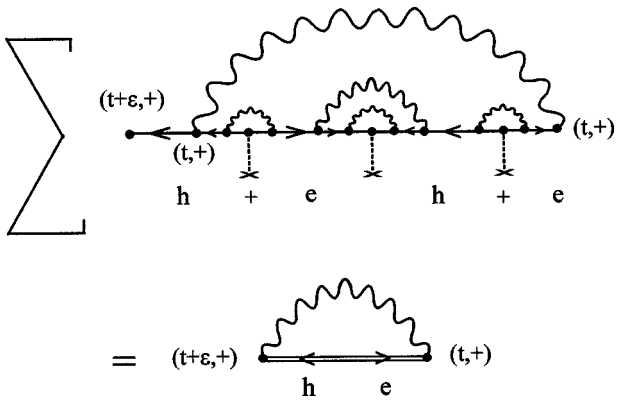

FIG. 17. Summation of Class (a23) graphs, in which the exposed V line ends in the end h segment. The graph shown on the left is a representative of the series.

(3) The remainder of the nonzero graphs give contributions from four-particle correlations. In this class of graphs, the exposed V line is crossed by at least one other V line. One consequence of the crossing is if that we remove the exposed V line, the graph is still connected. We further divide the class into four subsets by the particle label (e or h) of the exposed vertex and the particle label of the segment where the exposed V line terminates. Note that, by Rules 7 and 8, the exposed V line in this class can only end in either of the two middle segments. An example from each subset is shown in Fig. 18. We will prove the following claim.

Claim. The sum of each subset of graphs under consideration here can be factorized into a product of the exposed V line, $p_{eh}^{(1)*}$ and $\mathcal{B}_{eehh}^{(2)}$, the last being the $O(E^2)$ contribution to the nonsymmetrized biexcitonic correlation function [see Appendix B, Eq. (B2)].

We prove this claim only for the subset represented by Fig. 18(a). The same proof applies for the other three sub-

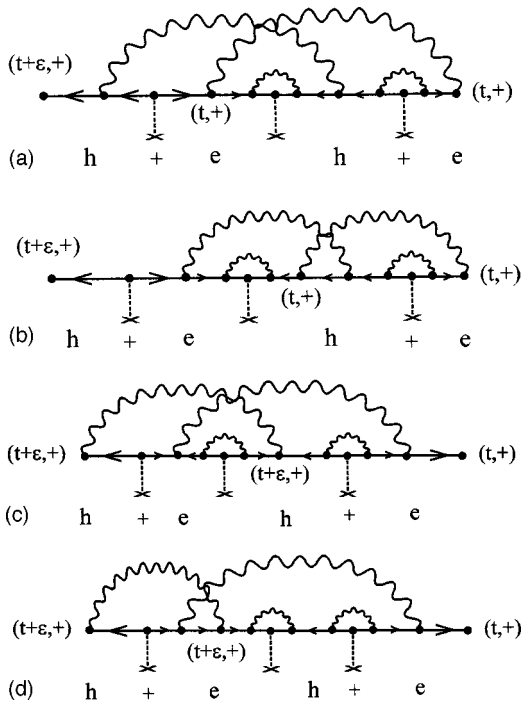

FIG. 18. Representatives of Class (a3) graphs.

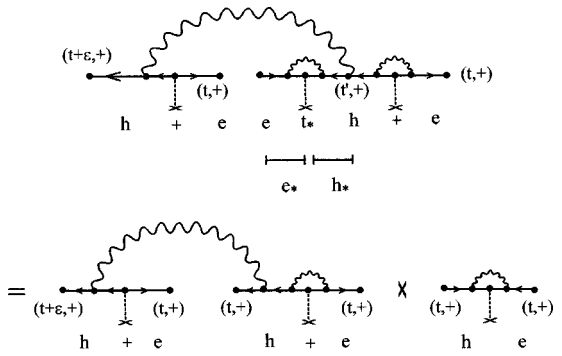

FIG. 19. Factorization of the graph in Fig. 18(a) with the exposed V-line removed into a product of graphs for $\mathcal{B}^{(2)}_{eehh}$ and $p^{(1)*}_{eh}$.

sets. We reproduce Fig. 18(a) in Fig. 19 with the exposed V line removed. The graph has two open particle chains with two E vertices and one E^* vertex. Assign the (Keldysh) time label $\bar{t}_*$ to the E^* vertex and the label e_* to the e segment bounded by the E^* vertex and the external point. Then, starting from the E^* vertex along the h segment in the other direction, label by $(t',+)$ the first V vertex, the V line from which ends in a segment other than e_*. Label by h_* the segment bounded by $\bar{t}_*$ and $(t',+)$. According to Rules 6, 7, and 9, $t'<t$, and all V lines starting in e_* end in the segment h_* since all V vertices in e_* lie either on the negative branch of the Keldysh contour or later than t on the positive branch. Consider the h line between $(t',+)$ and the next vertex on h_*, which we label $\bar{t}_1$. By factorizing this h line in the same way as in Eq. (11), we see that the graph is factorized into a $\mathcal{B}^{(2)}_{eehh}$ graph and a piece that would be a $p^{(1)*}_{eh}$ graph except for a more complicated Keldysh sign structure. We show in Appendix C that this complication generates extra terms that exactly cancel, as causality would demand, and the two-point graph in Fig. 19 is indeed a $p^{(1)*}_{eh}$ graph.

Since each graph in the set under consideration can be factorized in this way, and a graph assembled in the reverse manner from a V line, any $\mathcal{B}^{(2)}_{eehh}$ graph, and any $p^{(1)*}_{eh}$ graph obviously belongs to this set, the claim is proved. Including the contributions from the other three subsets, represented by Fig. 18(b–d), we obtain the sum of the whole class as

$$\begin{aligned} S_{a3}(i,j,t) = -\frac{i}{\hbar}\sum_{klmn}\,[&\langle il|V_{eeee}|km\rangle \\ &\times p^{(1)*}_{eh}(l,n,t)\mathcal{B}^{(2)}_{eehh}(k,m,j,n,t) \\ &+\langle il|V_{eheh}|km\rangle p^{(1)*}_{eh}(n,l,t)\mathcal{B}^{(2)}_{eehh}(k,n,j,m,t) \\ &+\langle jl|V_{hhhh}|km\rangle p^{(1)*}_{eh}(n,l,t)\mathcal{B}^{(2)}_{eehh}(i,n,k,m,t) \\ &+\langle jl|V_{hehe}|km\rangle p^{(1)*}_{eh}(l,n,t)\mathcal{B}^{(2)}_{eehh}(i,m,k,n,t)]. \end{aligned} \tag{16}$$

Class b. One particle chain and one loop. We divide this class into four subclasses:

(1) The exposed vertex is an E vertex (Fig. 20). In any such graph, the rest of the particle chain is a segment which is connected to the loop by V lines. All the graphs are then zero by Rule 8.

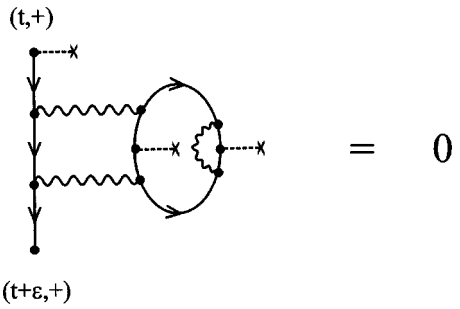

FIG. 20. A representative of Class (b1) graphs which all vanish.

(2) The exposed vertex is a V vertex, and the exposed V line ends on the open chain, not on the loop (Fig. 21). Again, by Rule 8, the segment between the end point of the exposed V line and the external point is an noninteracting particle line. By our convention of time ordering the external points, only the graphs in which the external line is an h line contribute. The result is

$$S_{b2}(i,j,t) = \frac{i}{\hbar}\sum_{mn}\langle ij|V_{eheh}|mn\rangle p^{(3b)}_{eh}(m,n,t), \tag{17}$$

where $p^{(3b)}_{eh}$ denotes that part of $p^{(3)}_{eh}$ that is given by graphs stemming from the bare graph in Fig. 13(b). $S_{a2}+S_{b2}$ gives the complete Fock mean-field contribution to the right-hand side of Eq. (13). Note that since $p^{(3a)}_{eh}+p^{(3b)}_{eh}=p^{(3)}_{eh}$, Eq. (13) is closed as far as the Fock terms are concerned.

(3) The exposed vertex is a V vertex, the exposed V line ends on the loop, and it is the only link between the loop and the open chain. These graphs give the Hartree mean-field contribution to the right hand side of Eq. (13). They vanish if the system is spatially uniform and electrically neutral overall since in this case the momentum transfer along the exposed V line must be zero, and this Fourier component of the Coulomb potential is excluded from the Hamiltonian. They do not, however, necessarily vanish in a more general setting. The graphs can again be grouped into four subsets by the particle labels of the end points of the exposed V line, and the sum of each subset can be expressed in closed form. A representative of each subset is shown in Fig. 22(a–d). The analytic expression of the sums can be written down by inspection as

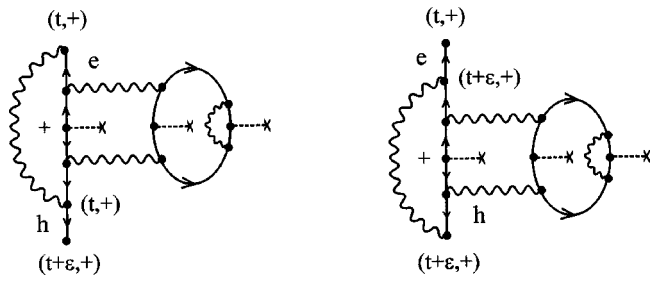

FIG. 21. Representatives of Class (b2) graphs.

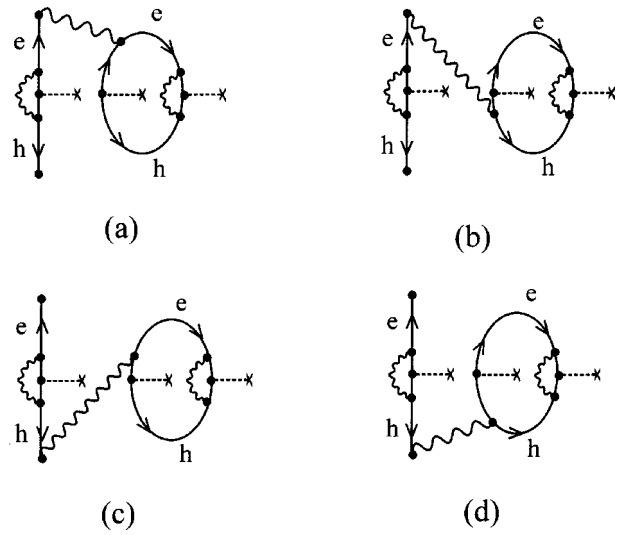

FIG. 22. Representatives of Class (b3) graphs.

$$S_{b3}(i,j,t)=\frac{i}{\hbar}\sum_{kmn}[\langle in|V_{eeee}|km\rangle f^{(2)}_{ee}(m,n,t)p^{(1)}_{eh}(k,j,t)$$
$$+\langle jn|V_{hhhh}|km\rangle f^{(2)}_{hh}(m,n,t)p^{(1)}_{eh}(i,k,t)$$
$$+\langle in|V_{eheh}|km\rangle f^{(2)}_{hh}(m,n,t)p^{(1)}_{eh}(k,j,t)$$
$$+\langle nj|V_{eheh}|mk\rangle f^{(2)}_{ee}(m,n,t)p^{(1)}_{eh}(i,k,t)]. \tag{18}$$

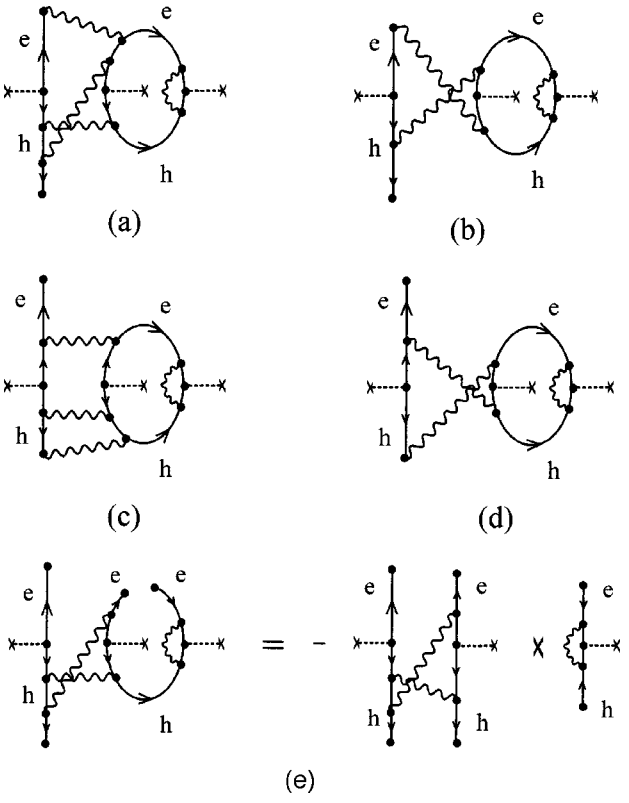

FIG. 23. (a)–(d) Representatives of Class (b4) graphs. (e) Factorization of the graph in (a) with the exposed V line removed into a product of graphs for $\mathcal{B}^{(2)}_{eehh}$ and $p^{(1)*}_{eh}$.

(4) The exposed vertex is a V vertex, the exposed V line ends on the loop, but the loop and the open chain are multiply connected. This class gives the correlation contributions, and its analysis parallels that for the class a(3) above. The graphs are again grouped into four subsets, an example of each is shown in Fig. 23. In Fig. 23(e), we show how one of the representative graphs, Fig. 23(a), is factorized into a biexcitonic correlation function and a $p^{(1)*}_{eh}$. The analytic expression for each subset is that of its counterpart in class a(3) with an ''exchanged'' correlation function: $\mathcal{B}^{(2)}_{eehh}(i,j,k,l,t)\rightarrow\mathcal{B}^{(2)}_{eehh}(i,j,l,k,t)$ and an extra minus sign due to the creation of the particle loop as a result of joining the three graphical elements. Thus the sum of the contributions from the present class and class a(3) is given by Eq. (16) with $-\mathcal{B}^{(2)}_{eehh}$ replaced by the antisymmetrized correlation function $b^{(2)}_{eehh}$. For clarity, we record this sum here, denoting it by S_4:

$$S_4(i,j,t)=\frac{i}{\hbar}\sum_{klmn}[\langle il|V_{eeee}|km\rangle$$
$$\times p^{(1)*}_{eh}(l,n,t)b^{(2)}_{eehh}(k,m,n,j,t)$$
$$+\langle il|V_{eheh}|km\rangle p^{(1)*}_{eh}(n,l,t)b^{(2)}_{eehh}(k,n,m,j,t)$$
$$+\langle jl|V_{hhhh}|km\rangle p^{(1)*}_{eh}(n,l,t)b^{(2)}_{eehh}(i,n,m,k,t)$$
$$+\langle jl|V_{hehe}|km\rangle p^{(1)*}_{eh}(l,n,t)b^{(2)}_{eehh}(i,m,n,k,t)]. \tag{19}$$

Summarizing, the equation of motion for $p^{(3)}_{eh}$, Eq. (13), can be written as

$$i\hbar\frac{d}{dt}p^{(3)}_{eh}(i,j,t)-\sum_{mn}[\epsilon_e(i,m)\delta_{jn}+\epsilon_h(j,n)\delta_{i,m}$$
$$+\langle ij|V_{eheh}|mn\rangle]p^{(3)}_{eh}(m,n,t)$$
$$=-i\hbar[S_{a1}(i,j,t)+S_{a21}(i,j,t)+S_{a22}(i,j,t)$$
$$+S_{b3}(i,j,t)+S_4(i,j,t)], \tag{20}$$

where the Pauli blocking terms S_{a1} are given by Eqs. (14), the Fock terms S_{a21},S_{a22} by Eq. (15), the Hartree terms S_{b3} by Eq. (18), and the correlation terms S_4 by Eq. (19). Note that we have moved the exciton interaction term $S_{a23}+S_{b2}$ [Eqs. (15) and (17)] to the left-hand side. Equation (20) is the $O(E^3)$ equation of motion for p_{eh} derived in DCT.

Finally, we note how some well-known angular-momentum selection rules can be easily deduced from the structures of the diagrams for $p^{(3)}_{eh}$.[17,23] We specialize to the case of one conduction band ($J_z=\pm\frac{1}{2}$) and one hole band ($J_z=\pm\frac{3}{2}$), where the two polarizations σ_+ and σ_- of the E field couple two separate sets of spin orbitals. Then we have the following simple rule which is valid to all orders in V and E: the polarization labels of all the $E(E^*)$ vertices along a continuous particle chain (open chain or loop) must be the same. We illustrate how this rule can be used for $p^{(3)}_{eh}$. Since the V vertices do not change the orbital spins, we only need to examine the bare graphs in Fig. 13. We can see then that in each Class a graph [Fig. 13(a)], all three $E(E^*)$ vertices

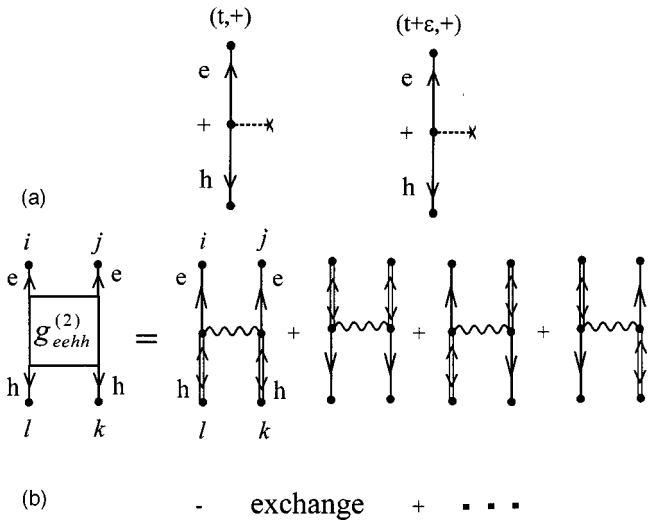

FIG. 24. (a) The bare graph for $b^{(2)}_{eehh}$. (b) Graphs of $g^{(2)}_{eehh}$ that contribute to the source terms in the equation for $b^{(2)}_{eehh}$.

have the same polarization sign. In a Class b graph [Fig. 13(b)], the E-E^* vertex pair on the loop must have the same polarization, which can, however, be different from that on the open chain. Take the example of two circularly polarized beams with opposite polarizations. Label the two fields E_+ and E_-. Only processes represented by Class b graphs contribute to $p^{(3)}_{eh}$ in this case. For the signal in the direction of E_+, corresponding to the combination $E_+E_-E_-^*$, E_-^*, and hence E_-, must be put on the loop, leaving E_+ to find its place on the open chain, which tells us that $p^{(3)}_{eh}$ has the polarization σ_+. In the four-wave-mixing directions, corresponding to $E_+E_+E_-^*$ and $E_-E_-E_+^*$, we see that neither can satisfy the rule that the E^* and the E on the loop have the same polarization sign. So there is no signal in these directions in this case.

D. $O(E^2)$ biexcitonic correlation graphs

In this subsection, we will derive the evolution equation of the two-electron–two-hole correlation function $b^{(2)}_{eehh}$, which appears in the source terms in the equation for $p^{(3)}_{eh}$ in the previous subsection. We again apply the inverses $G^{-1}_{e(0)}$ or $G^{-1}_{h(0)}$ to each of the four external lines and classify the graphs with an exposed vertex. The derivation here will be brief since most of the arguments are repetitions of those in previous subsections. We first note that, to $O(E^2)$, there is only one bare graph that is composed of two open chains with one E vertex on each [Fig. 24(a)]. This bare graph itself does not contribute to $b^{(2)}_{eehh}$; its connected dressed versions do. We also note that if the exposed vertex is an E vertex, the graph is zero by Rule 8.

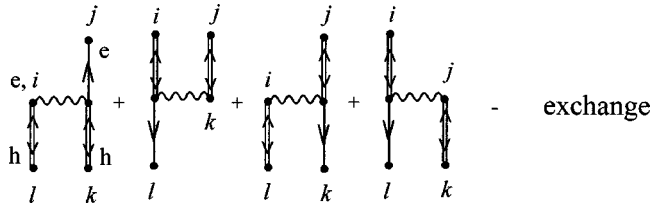

FIG. 25. Source terms in the equation for $b^{(2)}_{eehh}$, Eq. (21).

The source terms of the equation are given by graphs composed of two density functions $G_{\nu\nu}$, two polarization functions G_{eh}, and a V line linking the two chains. Since we are considering $O(E^2)$ graphs, these two-point functions must be $G_{\nu(0)}$ and $G^{(1)}_{eh}$. These graphs are shown in Fig. 24(b) where ''exchange'' refers to interchanging the orbital and time labels of the hole external points. Applying $G^{-1}_{\nu(0)}$ to the external particle lines of these graphs produces eight source terms which are shown graphically in Fig. 25 and are collected below on the right-hand side of Eq. (21). We next consider the remaining graphs, each with an external particle line removed. Suppose the exposed V line terminates in a particle segment labeled ν_*, which may be any one of the three segments other than the one from where the line originates. Since the termination point of the V line then carries the same time label as the external point of ν_*, by Rule 8 the subsegment between the two points must be a simple particle line $iG^{++}_{\nu(0)}$, which is equal to the identity in the orbital basis or 0 depending on the time ordering convention of the external points. If the exposed V line is removed, the remainder is again a graph contributing to $b^{(2)}_{eehh}$. It is then easy to see that all the nonzero graphs under consideration can be grouped into six terms, each of which is a product of the exposed V line and $b^{(2)}_{eehh}$ (Fig. 26). The equation of motion that results from the foregoing graphical analysis is

$$
\begin{aligned}
i\hbar\frac{d}{dt}b^{(2)}_{eehh}(i,j,k,l,t) &- \sum_{i'j'k'l'}[\epsilon_e(i,i')+\epsilon_e(j,j')+\epsilon_h(k,k')+\epsilon_h(k,k')]b^{(2)}_{eehh}(i',j',k',l',t)\\
&-\sum_{mn}\Big[\langle ij|V_{eeee}|mn\rangle b^{(2)}_{eehh}(m,n,k,l,t)+\langle ik|V_{eheh}|mn\rangle b^{(2)}_{eehh}(m,j,n,l,t)+\langle il|V_{eheh}|mn\rangle b^{(2)}_{eehh}(m,j,k,n,t)\\
&+\langle jk|V_{eheh}|mn\rangle b^{(2)}_{eehh}(i,m,n,l,t)\\
&=\sum_{mn}[\langle ij|V_{eeee}|mn\rangle\{p^{(1)}_{eh}(m,l,t)p^{(1)}_{eh}(n,k,t)-p^{(1)}_{eh}(m,k,t)p^{(1)}_{eh}(n,l,t)\}\\
&+\langle lk|V_{hhhh}|mn\rangle\{p^{(1)}_{eh}(i,m,t)p^{(1)}_{eh}(j,n,t)-p^{(1)}_{eh}(i,n,t)p^{(1)}_{eh}(j,m,t)\}+\{\langle ik|V_{eheh}|mn\rangle p^{(1)}_{eh}(m,l,t)\\
&-\langle il|V_{eheh}|mn\rangle p^{(1)}_{eh}(m,k,t)\}p^{(1)}_{eh}(j,n,t)+\{\langle jl|V_{eheh}|mn\rangle p^{(1)}_{eh}(m,k,t)\\
&-\langle jk|V_{eheh}|mn\rangle p^{(1)}_{eh}(m,l,t)\}p^{(1)}_{eh}(i,n,t)].
\end{aligned}
\tag{21}
$$

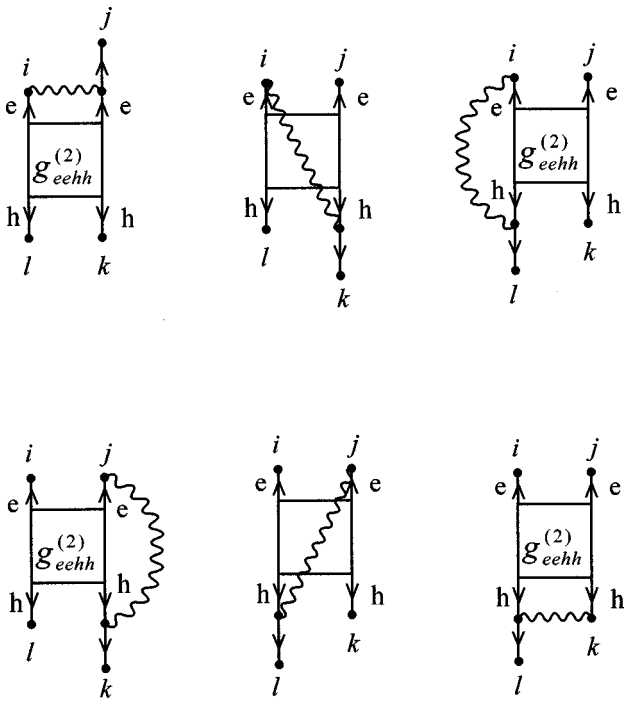

FIG. 26. Graphs representing interaction terms on the right-hand side of Eq. (21).

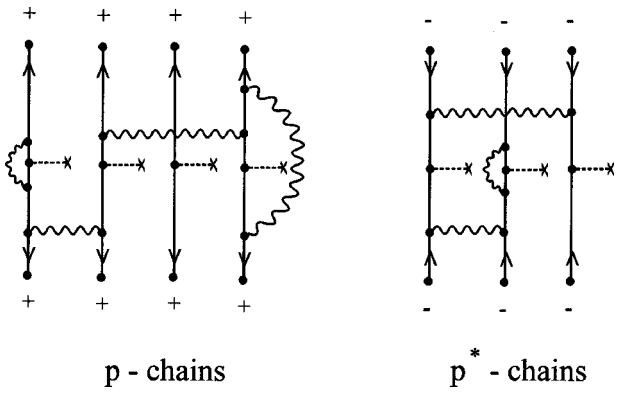

FIG. 27. An example of a minimal (E) order graph for a correlation function of an even number of creation operators and an even number of annihilation operators.

V. SUMMARY

In this paper, we have examined in details the perturbation series of the nonequilibrium Green's functions for an optically excited semiconductor system in the low-intensity limit. The purpose is to understand the connection between Green's function theory and the dynamic controlled truncation scheme for density matrices, which has been successful in this limit. By exploiting the well-recognized flexibility of the Green's function formalism, a comprehensive approach to semiconductor excitation dynamics may be developed in the future that incorporates features of DCT and is applicable to higher excitation intensities.

In the analysis, we have taken advantage of the diagrammatic representation of the perturbation series extensively. The crucial point is that the assumption of an initial ground state annihilates a vast class of diagrams. We classified the nonvanishing diagrams in increasing order of the external field. In each order up to order three, we showed that all nonvanishing terms (to arbitrary order in the two-particle interaction) contributing to the equal-time Green's functions —the density, the polarization, the biexcitonic correlation —can be resummed to yield closed equations of motions that have been derived within DCT. Corresponding to each term in the $\chi^{(3)}$ DCT equations, we have identified a class of Green's function graphs.

It is intended that, in future generalizations to higher intensities and/or nonzero initial densities, all these diagrams contributing to the $\chi^{(3)}$ DCT will be kept, and selected classes of other diagrams representing relevant high-density processes will be added in a ''consistent'' way. In the remainder of this section, we briefly comment on some directions for such generalizations. At higher intensities, the minimal order factorization theorems will be less and less relevant practically. In particular, Eq. (12) is no longer valid and the particle densities must be calculated by solving a dynamical equation, which can be derived diagrammatically in the form of a Dyson equation. Regrouping the graphs contributing to the interband polarization into a Dyson equation will also provide a proper treatment of dephasing due to carrier (exciton) -carrier (exciton) scattering. More important is that the biexcitonic correlations among two electrons and two holes are modified by the presence of other particles within the correlation range. Heuristically, we expect the four-body Hamiltonian in the equation of motion for b_{eehh} to be significantly modified by effects such as Pauli blocking, single-particle energy renormalizations (which consist of Hartree-Fock and time-nonlocal self-energy contributions) and collisional damping. In NGF, these effects are included by replacing each free-particle line in the graphs for b_{eehh} (see Figs. 18–26) by a full Green's function. In doing so, care must be taken to avoid double counting of graphs, which can be guaranteed by incorporating the biexcitonic correlations in the self-energy in the Dyson equation for the interband polarization. In this regard, we note that the ''noncrossing'' rule (Rule 9 in Sec. III) leads to a ladder structure for the interaction lines connecting the particle lines. Another relevant density effect is the screening of the two-particle interaction by density fluctuations. In NGF, screening is represented by a series of bubble diagrams. In the present case, two kinds of basic bubbles, namely, density and excitonic bubbles, contribute.

More generally, to include all the effects listed above, one needs a Dyson equation for the interband polarization whose self-energy, as a functional of the full Green's functions, includes the ladderlike graphs induced by the excitonic and biexcitonic correlations and the bubble screening graphs. In a future publication, we plan to make these ideas more explicit and to state detailed diagrammatic rules for them. Together with the present paper, we then hope to have laid the foundation for a more general treatment of correlation effects in nonequilibrium semiconductor dynamics.

ACKNOWLEDGMENTS

The support of JSOP, ARO, NSF, and COEDIP (University of Arizona) is gratefully acknowledged.

APPENDIX A

We show in this section that two general factorization results on a class of multipoint density matrices, which was derived in DCT,[2,3] can also be obtained quite easily from our

graphical considerations. Since the Hamiltonian conserves the number $N_e - N_h$, where N_e (N_h) is the number of electrons (holes), a density matrix of an odd number of creation/annihilation operators must vanish. For the density matrices of an even number of operators, we will prove the following claims.

Claim 1. The lowest-order (in the external field) contributions to a density matrix with M $a_e^\dagger(t)$'s, M $a_h^\dagger(t)$'s, N $a_e(t)$'s, and N $a_h(t)$'s contain M E vertices and N E^* vertices. To this minimal order, the density matrix factorizes as

$$\langle a^\dagger_{\nu_1}(i_1,t)\cdots a^\dagger_{\nu_{2M}}(i_{2M},t)a_{\nu_{2M+1}}(i_{2M+1},t)\cdots a_{\nu_{2(M+N)}}(i_{2(M+N)},t)\rangle$$
$$=\langle a^\dagger_{\nu_1}(i_1,t)\cdots a^\dagger_{\nu_{2M}}(i_{2M},t)\rangle\langle a_{\nu_{2M+1}}(i_{2M+1},t)\cdots a_{\nu_{2(M+N)}}(i_{2(M+N)},t)\rangle + O(E^{M+N+2}), \tag{A1}$$

where $\nu_k = e$ or h for $k=1,\ldots,2(M+N)$.

Claim 2. The lowest-order (in the external field) contributions to a density matrix with $M+1$ $a_e^\dagger(t)$'s, M $a_h^\dagger(t)$'s, $N+1$ $a_e(t)$'s, and N $a_h(t)$'s, contain $M+1$ E vertices and $N+1$ E^* vertices. To this minimal order, the density matrix factorizes as

$$\langle a^\dagger_{\nu_1}(i_1,t)\cdots a^\dagger_{\nu_{2M+1}}(i_{2M+1},t)a_{\nu_{2M+2}}(i_{2M+2},t)\cdots a_{\nu_{2(M+N+1)}}(i_{2(M+N+1)},t)\rangle$$
$$=\sum_j \langle a^\dagger_{\nu_1}(i_1,t)\cdots a^\dagger_{\nu_{2M+1}}(i_{2M+1},t)a_h^\dagger(j,t)\rangle\langle a_h(j,t)a_{\nu_{2M+2}}(i_{2M+2},t)\cdots a_{\nu_{2(M+N+1)}}(i_{2(M+N+1)},t)\rangle + O(E^{M+N+4}). \tag{A2}$$

An analogous result holds with e and h exchanged.

We have already proved two special cases of Claim 2: the factorization of the second-order density into two first-order polarizations in Sec. IV B ($M=0, N=0$) and the factorizations shown in Figs. 19 and 23(e) ($M=0$, $N=1$). To prove Claim 1, we note that the density matrix in question can be written as the equal-time limit of the $2(M+N)$-point Green's function

$$G^{N+,M-}_{\nu_1\cdots\nu_{2(M+N)}}(i_{2(M+N)},t_{2(M+N)},\ldots,i_1,t_1)$$
$$\equiv(-i)^{M+N}\langle T_-[a^\dagger_{\nu_{2M}}(i_{2M},t_{2M})\cdots a^\dagger_{\nu_1}(i_1,t_1)]T_+[a_{\nu_{2(M+N)}}(i_{2(M+N)},t_{2(M+N)})\cdots a_{\nu_{2M+1}}(i_{2M+1},t_{2M+1})]\rangle. \tag{A3}$$

Here all the annihilation operators are on the $+$ branch of the Keldysh contour and the creation operators are on the $-$ branch. To agree with the operator ordering in the density matrix, the time arguments approach the time t in the following orders: $t_{2M}>\cdots>t_1$ and $t_{2M+1}>\cdots>t_{2(M+N)}$. The Green's function can again be expanded diagrammatically following the rules in Appendix B and Sec. III. Each contributing graph contains $M+N$ open particle chains and a number of particle loops. The orbital and time labels of the creation/annihilation operators are assigned to the external points of the chains. We only consider the graphs with the minimal number of E (E^*) vertices. First, these graphs have no loops. Each open chain has at least one E (E^*) vertex on it, and this minimal number is obtained by pairing an $a_e^\dagger$ with an $a_h^\dagger$, or an a_e with an a_h, on each open chain. This proves the minimal contributing order is indeed $M+N$. Call an open chain with arrows pointing towards the external points (corresponding to annihilation operators) a p chain, and one with arrows pointing away from the external points (coresponding to creation operators) a p^* chain. Then the above considerations show that each minimal order graph, an example of which is shown in Fig. 27, consists of M p chains with positive Keldysh signs on their external points, N p^* chains with negative Keldysh signs on their external points, and an arbitrary number of V lines connecting the chains. Furthermore, an E vertex appear on each p chain, and one E^* vertex on each p^*-chain. Then, by Rule 5 in Sec. III, the Keldysh signs at all vertices on each such open chain must be the same as those on the chain's external points. This implies that no V lines can connect a p chain to a p^* chain: the graph is a product of two subgraphs, one with all the p chains and the other with all the p^* chains. The subgraph with the p-chains is a contributing minimal order graph to the factor density matrix with all annihilation operators in Eq. (A1), while that with the p^* chains contributes to minimal order to the factor density matrix with all creation operators. It is clear that the product of any pair of minimal order graphs from the two-factor density matrices is a minimal order graph of the origi

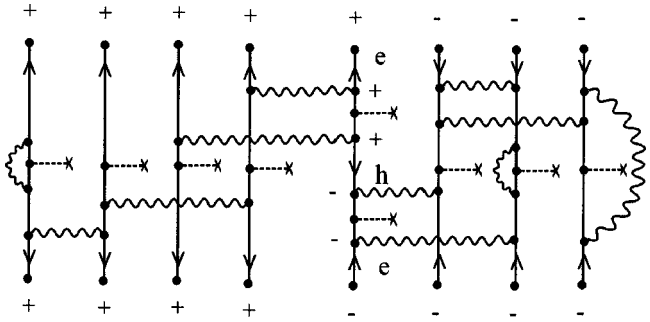

FIG. 28. An example of a minimal (E) order graph for a correlation function of an odd number of creation operators and an odd number of annihilation operators.

nal product density matrix [left-hand side of Eq. (A1)]. Claim 1 is thus proved.

A similar proof applies to Claim 2. Again the density matrix in question can be written as the equal-time limit of the $2(M+N+1)$-point Green's function

$$G^{(N+1)+,(M+1)-}_{\nu_1\cdots\nu_{2(M+N+1)}}(i_{2(M+N+1)},t_{2(M+N+1)},\ldots,i_1,t_1)$$
$$\equiv(-i)^{M+N+1}\langle T_-[a^\dagger_{\nu_{2M+1}}(i_{2M+1},t_{2M+1})\cdots a^\dagger_{\nu_1}(i_1,t_1)]$$
$$\times T_+[a_{\nu_{2(M+N+1)}}(i_{2(M+N+1)},t_{2(M+N+1)})\cdots a_{\nu_{2M+2}}(i_{2M+2},t_{2M+2})]\rangle. \quad \text{(A4)}$$

The time arguments approach the time t in the following orders: $t_{2M+1}>\cdots>t_1$ and $t_{2M+2}>\cdots>t_{2(M+N+1)}$. Here the number of open chains is $N+M+1$. Again each external point to which an arrow points (corresponding to an annihilation operator) is assigned a positive Keldysh sign, and a negative sign is assigned to each external point away from which an arrow is directed. To construct a minimal order graph, we again pair the operators to form as many p chains and p^* chains as possible. After M p chains and N p^* chains are assembled, the remaining pair of $a_e(t)$ and $a^\dagger_e(t)$ must form the last chain, which we will call an e chain, with a minimum of one E vertex plus one E^* vertex on it. So the minimal order for such density matrices is $M+N+2$. In a minimal order graph, e.g. Fig. 28, no V lines directly connect the sets of p and p^* chains, but both sets may be connected to the e chain. The (minimal order) e chain consists of two e segments separated by an h segment in the middle (Fig. 29). By Rules 5(b) and 5(c), the Keldysh signs at all points on the e segments are the same as those at the respective external points. The Keldysh signs on the h segment depend on the origins of the V lines that reach this segment. By Rule 5 (d), however, the positive signs and the negative signs must be segregated as shown in Fig. 29. The two h subsegments carrying opposite Keldysh signs are joined by a noninteracting h line, $iG^{-+}_{h(0)}$. We can now factorize this h line as in Eq. (11), thereby creating two h external points and factorizing the whole graph (Fig. 29). If we choose the time on the created h external points to approach t later than both t_{2M+1} and t_{2M+2}, we see that the factor graphs are minimal-order contributions to the respective factor density matrices in Eq. (A2). It is clear that any pair of minimal-order graphs from the two-factor density matrices assembled in the reverse manner will yield a minimal-order graph of the original product density matrix [left-hand side of Eq. (A2)]. Claim 2 is thus proved.

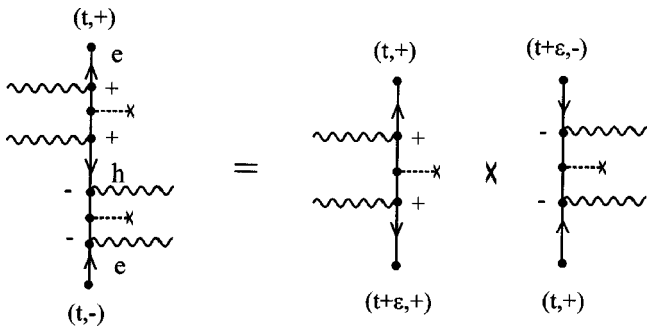

FIG. 29. Factorization of the (ee) chain in Fig. 28.

APPENDIX B: FEYNMAN RULES FOR GREEN'S FUNCTIONS

For notational clarity, we state the Feynman rules used in this paper for the time-dependent perturbation theory of the NGF's on the Keldysh time path. This set of rules is an extension to a two-component plasma of the standard one-component set stated in, e.g., Ref. 24. The derivation of these rules follows the general lines of argument for Green's functions perturbation theory as explained in, e.g., Ref. 16, and will not be given here. References 24 and 16 are the basic references for this appendix.

Our system is an electron-hole system governed by the Hamiltonian Eq. (1). We assume that, at the initial time t_0, the system is prepared in either a correlated, equilibrium state or an arbitrary but uncorrelated state. Wick's theorem is applicable to either case.[24] In the case of the initial equilibrium state with finite density, we assume the system has been left to equilibrate a long time before t_0. We further assume that the external field is switched on after t_0 and that the initial state is ''normal'' in the sense that in the absence of the external field, i.e., if $\hat{H}_{ext}(t)=0$, all the ''electron-hole-coherent'' Green's functions, e.g., $G_{eh}(i,\overline{t},j,\overline{t'})$ and $\tilde{G}_{eh}(i,\overline{t},j,\overline{t'})$, vanish. In this regard, we note that the interaction terms $\hat{H}_2$ in Eq. (1) conserve electron and hole numbers separately. The Keldysh time contour is shown in Fig. 2. The positive time branch from t_0 to ∞ is labeled C_+, the negative time branch is labeled C_-, and the entire contour is labeled C.

The Feynman rules for writing down the contributions, to nth order in the two-body interaction V and mth order in the external field E, to the two-point Green's functions

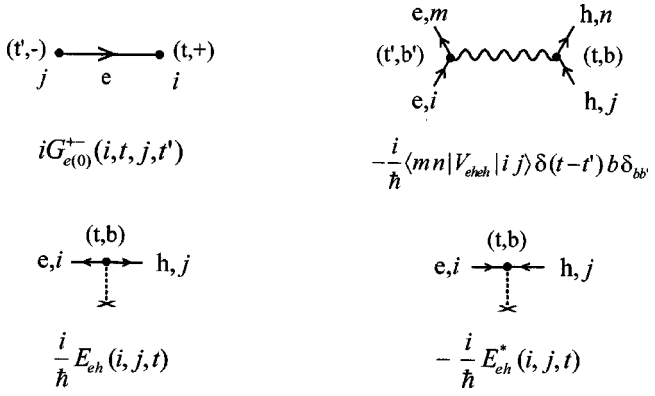

FIG. 30. Graphical elements in the perturbation theory used in this paper.

$iG_{\nu\nu'}(i,\bar{t},j,\bar{t'})$, defined in Eq. (2), are the following.

(B1) Draw all topologically distinct, connected diagrams with two external points, n interaction (or V) lines (denoted by wavy lines here), m external field (or E) lines (denoted by dashed lines), and $2n+m+1$ particle lines (denoted by directed solid lines). A V vertex is a vertex from which three lines emerge, two being particle lines and the third a V line. An E vertex is a vertex from which two particle lines and an E line emerge. Each V line begins and ends at V vertices. Each E line enters the diagram at only one E vertex. Each particle line is bounded by vertices or external points at both ends. These graphical elements are shown in Fig. 30 in which the labels (of time, orbital, etc.) and the corresponding analytical expressions, as given by the rules below, are also shown.

It is easy to see that in such a diagram the particle lines are arranged in a continuous chain running from one external point to the other and a number of nonoverlapping internal particle loops. Two successive lines along the open chain or a loop are joined by a vertex. In this paper, any continuous succession of alternating particle lines and vertices, with lines at the ends, is called a *chain*. A *segment* refers to a chain in which all the vertices are V vertices.

(B2) A particle line is labeled by either e, for electrons, or h, for holes. An orbital label is assigned to each end of the line. A time argument is assigned to each vertex, which is also labeled by the orbital and species labels of the particle lines emerging from it.

(B3) The two external points of the diagram are labeled by the time and orbital arguments of the Green's function. The arrow on the particle line connected to an external point is directed towards (away from) the point if the point is associated with an annihilation (creation) operator. For example, in a diagram contributing to $G_{ee}(i,\bar{t},j,\bar{t'})$, the arrow points towards $(i,\bar{t})$ and away from $(j,\bar{t'})$, while for $G_{eh}(i,\bar{t},j,\bar{t'})$, the arrow is directed towards the external point at both ends.

(B4) The arrow preserves its direction in successive particle lines until it meets an E vertex, where it switches to the opposite direction. The value of the particle label, e or h, is also preserved in successive particle lines until it meets an E vertex, where it switches to the other value.

We note that this rule is a result of our excluding the electron-hole pair creating or annihilating terms [Fig. 4(b)] from our interaction Hamiltonian $\hat{H}_2$. Including these processes would invalidate the rule. Some important consequences of the Feynman Rule (B4) are stated, as Rules 1–3, and proved in Sec. III. Also, it is obvious that all the particle lines in a segment, as defined below the Feynman Rule (B1), have the same arrow direction and species label.

For a given diagram, the analytic expression of the contribution is given by the following rules:

(B5) For each particle line with particle label ν and the arrow leading from a time-orbital label of $(\bar{t}_2,j)$ to $(\bar{t}_1,i)$, write down a factor $iG_{\nu(0)}(i,\bar{t}_1,j,\bar{t}_2)$, where $G_{\nu(0)}$ is the noninteracting Green's function.

(B6) For each V line, with orbitals m and i entering and exiting, respectively, a vertex labeled by time $\bar{t}_1$ and particle ν_1, and orbitals n and j entering and exiting, respectively, the other vertex, labeled by $\bar{t}_2$ and ν_2, assign the factor $-(i/\hbar)\langle ij|V_{\nu_1\nu_2\nu_1\nu_2}|mn\rangle\bar{\delta}(\bar{t}_1-\bar{t}_2)$, where

$$\bar{\delta}(\bar{t}_1-\bar{t}_2)=\begin{cases}\delta(t_1-t_2) & \text{if } \bar{t}_1,\bar{t}_2\in C_+\\ -\delta(t_1-t_2) & \text{if } \bar{t}_1,\bar{t}_2\in C_-\\ 0 & \text{elsewhere.}\end{cases}$$

(B7) For each E vertex, labeled by electron orbital i, hole orbital j, and time $\bar{t}$, assign a factor $(i/\hbar)E_{eh}(i,j,t)\equiv(i/\hbar)\mathbf{d}_{eh}(i,j)\cdot[\mathbf{E}(t)/2]e^{-i\omega_0 t}$ if both particle lines are exiting the vertex and a factor $-(i/\hbar)E^*_{eh}$ if both particle lines are entering the vertex. Note the difference in signs in the two cases. From here on, we call a vertex corresponding to E_{eh} an E vertex, and one corresponding to E^*_{eh} an E^* vertex.

(B8) Sum over all internal particle orbital labels, and integrate over all internal time variables along the Keldysh contour. The time integral is performed as a sum of the integrals on each branch of the contour: $\int_C d\bar{t}=\int_{t_0}^{\infty}dt_+ -\int_{t_0}^{\infty}dt_-$, where $t_\pm$ is the time variable on the branch $C_\pm$.

(B9) Attach a sign factor of $(-1)^{N_l}$ where N_l is the number of particle loops in the diagram.

The exact Green's functions are denoted by double solid lines (Fig. 31), which are labeled at both ends by time, species, and orbital arguments.

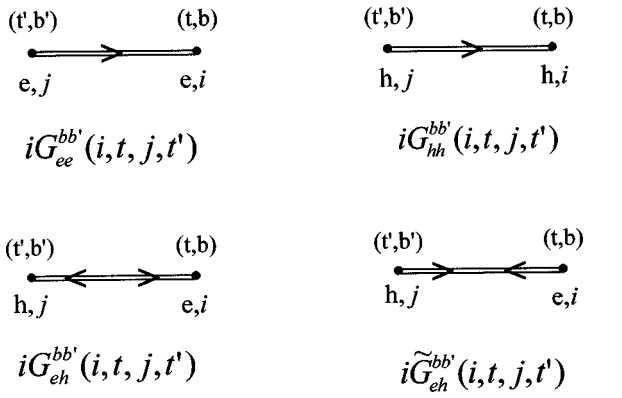

FIG. 31. Graphical representations of the exact two-point Green's functions.

Each Green's function may alternatively be written as a four-component function (or 2×2 matrix) labeled by two ''Keldysh signs'' and depending on two time ordinary time variables: e.g., $G^{bb'}_{ee}(i,t,j,t'),b,b'=\pm$ and $t,t'\in C_+$. This change in convention leads to some slight modifications of the above rules. Each particle line is now labeled by a time Keldysh sign pair (t,b) at each end, and so are a vertex and an external point. The factor associated with a V line is now $-(i/\hbar)\langle ij|V_{\nu_1\nu_2\nu_1\nu_2}|mn\rangle\delta(t_1-t_2)b_1\delta_{b_1b_2}$, the notations being those in the Feynman Rule (B6) above. At each internal vertex, labeled by the orbital labels (i,j), the time argument t_1 and Keldysh sign b_1 perform the following sums and integral: $\Sigma_{ij}\int_{t_o}^{\infty}\Sigma_{b_1}b_1\cdots$.

The perturbation series for the four-point function $G_{eehh}(i,\bar{t},j,\bar{t'},k,\bar{t''},l,\bar{t'''})$ can be written down by the above Feynman rules with the following differences:

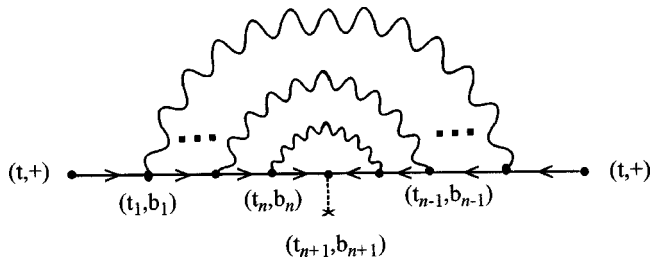

FIG. 32. A graph that differs from a representative graph for $p_{eh}^{(1)*}$ of the same order in V only by the Keldysh signs at the end points.

(B10) A graph to order n in V and order m in E (E^*) has $2n+m+2$ particle lines, which are arranged into two open chains and a number of internal loops. The two open chains need not be connected to each other, but an internal loop must be connected to at least one of the two chains.

(B11) With the above ordering of the orbital labels (i,j,k,l) for the external points, an extra minus sign is assigned to a graph in which i and k are the external points of one chain, and j and l are those of the other.

One can isolate those graphs that are factorizable into products of two G_{eh}'s and write

$$G_{eehh}(i,\overline{t},j,\overline{t'},k,\overline{t''},l,\overline{t'''}) = G_{eh}(i,\overline{t},l,\overline{t'''})G_{eh}(j,\overline{t'},k,\overline{t''}) - G_{eh}(i,\overline{t},k,\overline{t''})G_{eh}(j,\overline{t'},l,\overline{t'''}) + g_{eehh}(i,\overline{t},j,\overline{t'},k,\overline{t''},l,\overline{t'''}), \tag{B1}$$

where g_{eehh}, the correlated part of G_{eehh}, is composed of graphs in which the open chains are also connected to each other. The antisymmetry of g_{eehh} under electron or hole exchange is obvious from the graphical expansion. As a result, we can write g_{eehh} in terms of a nonsymmetrized function:

$$g_{eehh}(i,\overline{t},j,\overline{t'},k,\overline{t''},l,\overline{t'''}) = \mathcal{G}_{eehh}(i,\overline{t},j,\overline{t'},k,\overline{t''},l,\overline{t'''}) - \mathcal{G}_{eehh}(i,\overline{t},j,\overline{t'},l,\overline{t'''},k,\overline{t''}), \tag{B2}$$

where $\mathcal{G}_{eehh}(i,\overline{t},j,\overline{t'},k,\overline{t''},l,\overline{t'''})$ is the sum of all those graphs in $g_{eehh}(i,\overline{t},j,\overline{t'},k,\overline{t''},l,\overline{t'''})$ in which $(i,\overline{t})$ is paired with $(l,\overline{t'''})$, and $(j,\overline{t'})$ with $(k,\overline{t''})$, in the open chains. In the equal-time limit, g_{eehh}^{++++} and $\mathcal{G}_{eehh}^{++++}$ define the antisymmetrized correlation function b_{eehh} and nonsymmetrized correlation function $\mathcal{B}_{eehh}$, respectively.

APPENDIX C

In this appendix, we prove that the sum of all two-point graphs, each carrying one E^* vertex and Keldysh-time assignment $(t,+)$ at both ends, is equal to $p_{eh}^{(1)*}$, as is claimed in Sec. IV C. We show a representative of the graphs, with n V lines, in Fig. 32. Comparing this graph with Fig. 10, we see that it the same as the graph from $p_{eh}^{(1)*}$ with the same number of V lines except that in Fig. 32, the Keldysh signs at the two end points are $+$, and a sum is performed over the Keldysh signs at the V vertices. The claim is, despite this

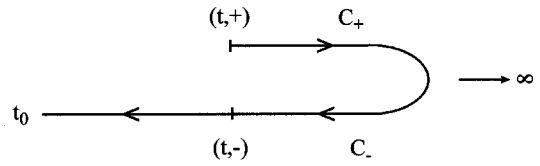

FIG. 33. Keldysh contours showing respective time integration ranges for the graphs in Figs. 10 and 32.

difference, that the two series yield the same analytical expression order by order in V. The plausibility of this claim can be seen by a heuristic causality argument. The difference between the two graphs in question is a difference in the integration ranges over the Keldysh contour (Fig. 33). For the graph in Fig. 32, the integration range starts at $(t,+)$ and goes along C_+ to ∞ and then back along C_- to t_0, while for the corresponding graph in Fig. 10, the integration goes from $(t,-)$ to t_0. Since events happening to the system at times later than t should not affect the correlation functions at t, we expect the net contribution from the part of the contour between $(t,+)$ and $(t,-)$ to vanish. In the following, we give a formal proof of the claim.

We can write the expression corresponding to the graph that ends at $(t,+)$ in the form [cf. Eq. (7)]

$$\int_{-\infty}^{\infty} dt dt_1 \ldots dt_{n+1}\theta(t,t_1,\ldots,t_{n+1})F(t,t_1,\ldots,t_{n+1}),$$

where $\theta(t,t_1,\ldots,t_{n+1})$ contains a sum of products of step functions in time corresponding to various combinations of Keldysh signs, and $F(t,t_1,\ldots,t_{n+1})$ contains factors of $-ie^{-(i/\hbar)\epsilon_\nu(t-t')}$ and V and is free of Kelysh signs. To figure out the form of $\theta(t,t_1,\ldots,t_{n+1})$, we note that by Rule 5(d), in each allowed combination, the positive signs and the negative signs must be segregated. We show a particular combination in Fig. 34, in which the sign switches from positive at t_m to negative at t_{m+1}. This gives rise to a factor of $(-1)^{n+1-m}\theta(t_1-t)\theta(t_2-t_1)\cdots\theta(t_m-t_{m-1})\theta(t_{m+1}-t_{m+2})\cdots\theta(t_n-t_{n+1})$. Summing over all allowed combinations, we can write the result compactly as

$$\theta(t,t_1,\ldots,t_{n+1}) = \sum_{m=0}^{n+1}(-1)^{n+1-m} \times \prod_{k=1}^{m}\theta(t_k-t_{k-1}) \times \prod_{j=m+1}^{n}\theta(t_j-t_{j+1}), \tag{C1}$$

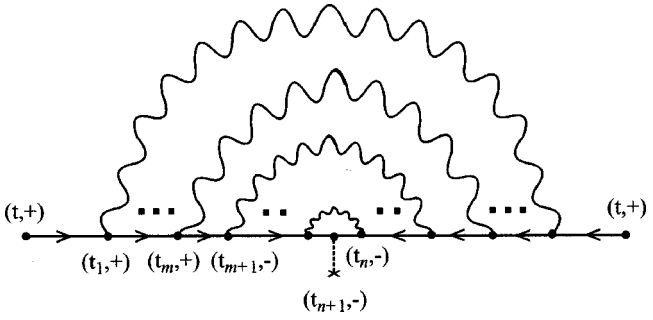

FIG. 34. A particular combination of Keldysh signs for the intermediate vertices in Fig. 32.

where t has been relabeled t_0. Any product in Eq. (C1) is set equal to 1 if the lower limit exceeds the upper limit [e.g., $\Pi_{j=m+1}^{n}\theta(t_j-t_{j+1})=1$ if $m+1>n$]. The expression for the graph from $p_{eh}^{(1)*}$ can also be written in the same form with the same $F(t,t_1,\ldots,t_{n+1})$ but with $\theta(t,t_1,\ldots,t_{n+1})$ replaced by

$$(-1)^{n+1}\prod_{j=0}^{n}\theta(t_j-t_{j+1}). \tag{C2}$$

The claim is thus reduced to the statement that Eqs. (C1) and (C2) are equal.

We will prove the claim by induction. First it is easy to check that the claim is true for $n=1$ and $n=2$. Suppose the claim is true for $n=N$, i.e.,

$$\sum_{m=0}^{N+1}(-1)^{N+1-m}\prod_{k=1}^{m}\theta(t_k-t_{k-1})\prod_{j=m+1}^{N}\theta(t_j-t_{j+1}) =(-1)^{N+1}\prod_{j=0}^{N}\theta(t_j-t_{j+1}). \tag{C3}$$

Consider the case $n=N+1$. The right-hand side is

$$\sum_{m=0}^{N+2}(-1)^{N+2-m}\prod_{k=1}^{m}\theta(t_k-t_{k-1})\prod_{j=m+1}^{N+1}\theta(t_j-t_{j+1}). \tag{C4}$$

We separate out the $m=0$ term and make the substitutions $m'=m-1$, $k'=k-1$, $j'=j-1$ to turn the expression into

$$\theta(t_1-t_0)\sum_{m'=0}^{N+1}(-1)^{N+1-m'}\prod_{k'=1}^{m'}\theta(t_{k'+1}-t_{k'}) \times\prod_{j'=m'+1}^{N}\theta(t_{j'+1}-t_{j'+2})+(-1)^{N+2}\prod_{j=1}^{N+1}\theta(t_j-t_{j+1}). \tag{C5}$$

We see that the first term, without the factor $\theta(t_1-t_0)$, is just the right-hand side of Eq. (C3) if we replace $t_{k'}$ by $t_{k'-1}$ and $t_{j'}$ by $t_{j'-1}$. Since Eq. (C3) is a formal identity for the set $(t_0,t_1,\ldots,t_{N+1})$, it is also valid for the set $(t_1,t_2,\ldots,t_{N+1})$. Thus Eq. (C5) can be written as

$$\theta(t_1-t_0)(-1)^{N+1}\prod_{j=1}^{N+1}\theta(t_j-t_{j+1})+(-1)^{N+2} \times\prod_{j=1}^{N+1}\theta(t_j-t_{j+1}) =(-1)^{N+2}\prod_{j=1}^{N+2}\theta(t_j-t_{j+1}). \tag{C6}$$

Thus the claim is true for all n.

[1] V.M. Axt and A. Stahl, Z. Phys. B: Condens. Matter **93**, 195 (1994).

[2] M. Lindberg, Y.Z. Hu, R. Binder, and S.W. Koch, Phys. Rev. B **50**, 18 060 (1994).

[3] K. Victor, V.M. Axt, and A. Stahl, Phys. Rev. B **51**, 14 164 (1995).

[4] V.M. Axt, K. Victor, and T. Kuhn, Phys. Status Solidi B **206**, 189 (1998).

[5] G. Bartels, A. Stahl, V. Axt, B. Haase, U. Neukrich, and J. Gutowski, Phys. Rev. Lett. **81**, 5880 (1998).

[6] P. Kner, S. Bar-Ad, M.V. Marquezini, D.S. Chemla, and W. Schäfer, Phys. Rev. Lett. **78**, 1319 (1997).

[7] W. Schäfer, D. Kim, J. Shah, T. Damen, J. Cunningham, K. Goossen, L. Pfeiffer, and K. Köhler, Phys. Rev. B **53**, 16 429 (1996).

[8] W. Schäfer and M. Wegener, *Semiconductor Optics and Transport—from Fundamentals to Current Topics* (Springer, Berlin, in press).

[9] H. Haug and S. Schmitt-Rink, Prog. Quantum Electron. **9**, 3 (1984).

[10] R. Zimmermann, *Many-Particle Theory of Highly Excited Semiconductors* (Teubner, Leipzig, 1988).

[11] W. Schäfer and J. Treusch, Z. Phys. B: Condens. Matter **63**, 407 (1986).

[12] R. Binder and S. Koch, Prog. Quantum Electron. **19**, 307 (1995).

[13] H. Haug and A. P. Jauho, *Quantum Kinetics in Transport and Optics of Semiconductors* (Springer, Berlin, 1996).

[14] W. Pötz, Phys. Rev. B **54**, 5647 (1996).

[15] L. P. Kadanoff and G. Baym, *Quantum Statistical Mechanics* (Addison-Wesley, New York, 1989).

[16] A. Fetter and J. Walecka, *Quantum Theory of Many-Particle Systems* (McGraw-Hill, New York, 1971).

[17] M.Z. Maialle and L.J. Sham, Phys. Rev. Lett. **73**, 3310 (1994).

[18] M. Z. Maialle, Ph.D. thesis, Department of Physics, University of California, San Diego, 1994.

[19] A. Stahl, Z. Phys. B: Condens. Matter **72**, 371 (1988).

[20] V. Axt and S. Mukamel, Rev. Mod. Phys. **70**, 145 (1998).

[21] Th. Östreich, K. Schönhammer, and L.J. Sham, Phys. Rev. Lett. **74**, 4698 (1995).

[22] Th. Östreich, K. Schönhammer, and L.J. Sham, Phys. Rev. B **58**, 12 920 (1998); cond-mat/9807127.

[23] M. Lindberg, R. Binder, Y.Z. Hu, and S.W. Koch, Phys. Rev. B **49**, 16 942 (1994).

[24] P. Danielewicz, Ann. Phys. (N.Y.) **152**, 239 (1984).